Iron depletion in the deep chlorophyll maximum: mesoscale eddies as natural iron fertilization experiments

Nicholas J. Hawco[1], Benedetto Barone[2], Matthew J Church[3], Lydia Babcock-Adams[4], Daniel J Repeta[4], Emma Wear[3], Rhea K Foreman[5], Karin M. Björkman[2], Shavonna Bent[4], Benjamin A.S. Van Mooy[4], Uri Sheyn[2], Edward F. DeLong[6], Marianne Acker[4], Rachel L. Kelly[7], Alex Nelson[8], John Ranieri[3], Tara Clemente[2], David M Karl[9], and Seth G John[7]

[1]University of Hawaii at Mānoa
[2]University of Hawaii at Manoa
[3]University of Montana
[4]Woods Hole Oceanographic Institution
[5]University of Hawaii - Manoa
[6]University of Hawaii
[7]University of Southern California
[8]University of Hawaii Manoa
[9]Department of Oceanography, University of Hawaii, Honolulu, HI 96822, USA

November 23, 2022

Abstract

In stratified oligotrophic waters, phytoplankton communities forming the deep chlorophyll maximum (DCM) are isolated from atmospheric iron sources above and remineralized iron below. Reduced supply leads to a minimum in dissolved iron (dFe) near 100 m, but it is unclear if iron limits growth at the DCM. Here, we propose that natural iron addition events occur regularly with the passage of mesoscale eddies, which alter the supply of dFe and other nutrients relative to the supply of light, and can be used to test for iron limitation at the DCM. This framework is applied to two eddies sampled in the North Pacific Subtropical Gyre. Observations in an anticyclonic eddy center indicated downwelling of iron-rich surface waters, leading to increased dFe at the DCM but no increase in productivity. In contrast, uplift of isopycnals within a cyclonic eddy center increased supply of both nitrate and dFe to the DCM, and led to dominance of picoeukaryotic phytoplankton. Iron addition experiments did not increase productivity in either eddy, but did enhance leucine incorporation at ambient light in the cyclonic eddy, a potential indicator of iron stress among *Prochlorococcus*. Rapid cycling of siderophores and low dFe:nitrate uptake ratios also indicate that a portion of the microbial community was stressed by low iron. However, near-complete nitrate drawdown in this eddy, which represents an extreme case in nutrient supply compared to nearby Hawaii Ocean Time-series observations, suggests that recycling of dFe in oligotrophic ecosystems is sufficient to avoid iron limitation in the DCM under typical conditions.

Iron depletion in the deep chlorophyll maximum: mesoscale eddies as natural iron fertilization experiments

Nicholas J. Hawco[1,2], Benedetto Barone[2], Matthew J. Church[3], Lydia Babcock-Adams[4], Daniel J. Repeta[4], Emma K. Wear[3], Rhea K. Foreman[2], Karin M. Björkman[2], Shavonna Bent[4], Benjamin A. S. Van Mooy[4], Uri Sheyn[2], Edward F. Delong[2], Marianne Acker[4], Rachel L. Kelly[1], Alex Nelson[2], John Ranieri[3], Tara M. Clemente[2], David M. Karl[2], and Seth G. John[1]

[1]Department of Earth Sciences, University of Southern California, Los Angeles, CA, USA

[2]Department of Oceanography, University of Hawai‘i at Mānoa, Honolulu, HI, USA

[3]Flathead Lake Biological Station, University of Montana, Polson, MT, USA

[4]Woods Hole Oceanographic Institution, Woods Hole, MA, USA

Corresponding author: Nicholas Hawco (hawco@hawaii.edu)

Key Points:

- Both cyclonic and anticyclonic eddies add iron to the lower euphotic zone of oligotrophic gyres.
- In an anticyclonic eddy, dissolved iron at the deep chlorophyll maximum increased but productivity did not.
- Uptake of upwelled iron and nitrate in a cyclonic eddy led to low iron conditions and stress, but did not limit productivity.

Abstract

In stratified oligotrophic waters, phytoplankton communities forming the deep chlorophyll maximum (DCM) are isolated from atmospheric iron sources above and remineralized iron below. Reduced supply leads to a minimum in dissolved iron (dFe) near 100 m, but it is unclear if iron limits growth at the DCM. Here, we propose that natural iron addition events occur regularly with the passage of mesoscale eddies, which alter the supply of dFe and other nutrients relative to the supply of light, and can be used to test for iron limitation at the DCM. This framework is applied to two eddies sampled in the North Pacific Subtropical Gyre. Observations in an anticyclonic eddy center indicated downwelling of iron-rich surface waters, leading to increased dFe at the DCM but no increase in productivity. In contrast, uplift of isopycnals within a cyclonic eddy center increased supply of both nitrate and dFe to the DCM, and led to dominance of picoeukaryotic phytoplankton. Iron addition experiments did not increase productivity in either eddy, but did enhance leucine incorporation at ambient light in the cyclonic eddy, a potential indicator of iron stress among *Prochlorococcus*. Rapid cycling of siderophores and low dFe:nitrate uptake ratios also indicate that a portion of the microbial community was stressed by low iron. However, near-complete nitrate drawdown in this eddy, which represents an extreme case in nutrient supply compared to nearby Hawaii Ocean Time-series observations, suggests that recycling of dFe in oligotrophic ecosystems is sufficient to avoid iron limitation in the DCM under typical conditions.

1 Introduction

Approximately 30% of the ocean's surface is subject to phytoplankton iron (Fe) limitation, especially in the Equatorial Pacific and Southern Oceans where upwelling provides a large flux of nitrate (NO_3^-) and other nutrients (Moore et al., 2013; Moore et al., 2001). Elsewhere, stratification of the upper ocean leads to depletion of NO_3^-, ammonia, and other bioavailable forms of nitrogen. In stratified oligotrophic gyres, shallow mixed layers also act to concentrate Fe deposited at the ocean's surface by atmospheric sources (Boyle et al., 2005; Sedwick et al., 2005). The large flux of Fe relative to NO_3^- in these ecosystems results in nitrogen limitation of photosynthesis and selects for phytoplankton like the cyanobacterium *Prochlorococcus* (Ward et al., 2013; Wu et al., 2000), whose small size allows them to outcompete other phytoplankton for recycled nitrogen species found at nanomolar concentrations (Morel et al., 1991).

However, the same stratification that leads to Fe-rich conditions in the surface ocean can also impede Fe supply to the subsurface. Shallow mixed layers ensure that Fe derived from dust deposition does not reach the entirety of the euphotic zone, which can extend below 100 m in subtropical gyres. Stratification also limits the supply of regenerated Fe from below the euphotic zone. Indeed, a common feature of dFe profiles within subtropical gyres is a concentration minimum between 75-150 m (Bruland et al., 1994; Fitzsimmons et al., 2015; Sedwick et al., 2005). This subsurface dFe minimum often coincides with the deep chlorophyll maximum (DCM), a unique habitat where low irradiance drives phytoplankton photo-acclimation, increasing chlorophyll per cell to improve photosynthetic light capture (Letelier et al., 2004). Theoretical arguments suggest the increases in chlorophyll per cell must be matched by an

equivalent increase in the number of Fe-bearing photosynthetic reaction centers, increasing cellular Fe requirements substantially (Raven, 1990; Sunda & Huntsman, 1997).

The combination of low Fe supply and high demand allows dFe in the DCM of the North Pacific Subtropical Gyre to fall below 100 pM, similar to dFe measured in the Fe-limited Equatorial Pacific and Southern Ocean (Coale et al., 1996; Martin et al., 1990). It is unclear if the growth of phytoplankton in the DCM is limited at these concentrations. Classical explanations of the DCM emphasize the optimization of opposing gradients in light and nutrient flux without invoking Fe specifically (Cullen, 2015; Letelier et al., 2004). This balance is borne out in the seasonal cycle at Station ALOHA, a site that is broadly representative of the North Pacific Subtropical Gyre (Karl et al., 2021). Increasing light intensity from winter to summer allows the DCM to deepen into the nutricline, which enhances NO_3^- uptake and increases phytoplankton biomass (Letelier et al., 2004). In both seasons, the DCM is positioned at a similar light flux: roughly 0.5 mol photon m^{-2} day^{-1}, a threshold that has also been identified in other oligotrophic regions (Mignot et al., 2014), implying a fundamental control by light. However, recent experiments in the California Current Ecosystem have shown that eukaryotic phytoplankton in the DCM, especially diatoms, respond more strongly to concurrent increases in both Fe and light, compared to increases in light alone, suggesting that Fe limitation may influence productivity in this region (Hogle et al., 2018; Hopkinson & Barbeau, 2008). From this perspective, it may be significant that the seasonal deepening of the DCM at Station ALOHA coincides with a springtime increase in Fe supply from Asian dust (Boyle et al., 2005).

Definitive evidence of Fe limitation in surface waters ultimately demanded the upscaling of Fe addition experiments from liter-sized bottles to the ecosystem scale via *in situ* fertilization experiments (Boyd et al., 2007), and from parallel studies of natural iron fertilization events:

coastal Fe input from islands (Blain et al., 2007; Martin et al., 1994; Pollard et al., 2009), or atmospheric deposition from dust storms (Bishop et al., 2002) and volcanic eruptions (Achterberg et al., 2013; Hamme et al., 2010). At present, there are significant logistical (not to mention ethical (Strong et al., 2009)) challenges facing would-be Fe fertilization experiments in the lower euphotic zone: the DCM cannot be observed by satellite and is out of reach of most underway sampling systems. Natural Fe fertilization events to the oligotrophic DCM (if they can be observed) represent an alternate approach.

Here, we show how perturbations to light, nutrient and iron supply caused by mesoscale eddy activity can be used to examine the vulnerability of phytoplankton in the DCM to iron limitation. This scheme is then applied to two adjacent eddies, a cyclone and an anticyclone, observed in the North Pacific Subtropical Gyre during Summer 2017. Along with several recent studies (Browning et al., 2021; Ellwood et al., 2020; Sedwick et al., 2020), our measurements show that local Fe cycling is strongly perturbed by mesoscale eddies.

2 Methods

2.1 Expedition summary

Sampling and experiments were conducted on the R/V *Kilo Moana* as part of the MESO-SCOPE expedition (June 26 – July 15, 2017) in the North Pacific Subtropical Gyre. Satellite altimetry was accessed from the Copernicus Marine Environmental Monitoring Service (CMEMS) and processed as described by Barone et al. (2019) to remove the seasonal cycle and interannual trend. The centers of the two mesoscale eddies sampled in this study were identified as maxima and minima of corrected sea level anomaly (SLA_{corr}): a cyclonic eddy centered at 24.9ºN, 158.7ºW, and an anticyclonic eddy centered at 26.4ºN, 158.0ºW. An initial survey of the

subsurface density structure across the upper water column was performed with an underway CTD (Teledyne), followed by hydrographic sampling for metals and nutrients, and deployment of autonomous Wirewalker drifting profilers near the eddy centers. This initial sampling was followed by Lagrangain, multi-day occupations of the eddy centers following Surface Velocity Program (SVP) drifters tracking near surface currents at 15 m depth, deployed near the centers of both eddies. Two Wirewalker drifting profilers were deployed near the SVP drifters to obtain vertically resolved observations of the upper 400 m at high temporal resolution. A more detailed descriptin of sampling activities can be found in a companion manuscript (Barone et al., Submitted). During the Lagrangian period, three 12-hr primary production experiments were conducted in each eddy using surface tethered arrays following established methods for the Hawaii Ocean Time-series (HOT). These were accompanied by a longer term (88-hr) Fe amendment experiments on a separate array.

For all hydrographic parameters, sampling depths were converted to a mean isopycnal depth specific to each eddy center, which was calculated based on multi-day averages of potential density profiles determined from the Wirewalkers. Daily integrals of downwelling photosynthetically active radiation (PAR) were calculated as the product of continuous measurements of surface PAR from a shipboard sensor (LI-COR LI-190), and the attenuation of PAR with depth, measured daily with a Hyperpro II optical profiler (Sea-Bird). Reported PAR values at the DCM are averaged from 5 m above and below the mean isopycnal depth of the DCM for each day, and then averaged across the 3 day Lagrangian sampling period.

2.2 Nutrient, chlorophyll, and flow cytometry analyses

Nutrient samples were collected using a rosette sampler and frozen immediately. Concentrations of nitrate + nitrite were analyzed by the high sensitivity chemiluminescent

141 method described by Foreman et al. (2016), with a detection limit of 1 nM. Individual samples
142 near the DCM of both eddies were also analyzed for nitrite using chemiluminescence (Foreman
143 et al., 2016). Dissolved silicate was measured colometrically using a SEAL AA3 auto-analyzer
144 (Strickland & Parsons, 1972; Wilson et al., 2019). Chlorophyll *a* was measured by the
145 fluorometric method after acetone extraction (Lorenzen, 1967). Abundance of divinyl
146 chlorophyll *a* and *b* were measured by high performance liquid chromatography mass
147 spectrometry (HPLC-MS) following procedures recently described by Becker et al. (2021).
148 Abundance of picoeukaryotes, *Prochlorococcus*, and heterotrophic bacterial cells were preserved
149 in 0.24% paraformaldehyde, flash frozen at -80 °C and analyzed by flow cytometry on an Influx
150 flow cytometer (Cytopeia). Phytoplankton populations were identified by fluorescence and
151 scattering properties. Heterotrophic (non-pigmented) populations were analyzed after staining
152 with SYBER Green I, with phytoplankton contributions subtracted.

153 *2.3 Dissolved iron sampling and analysis*

154 Trace metal sampling was conducted using a 12-position powder-coated 'trace metal'
155 rosette (SBE 32C with SBE 9plus CTD, Sea-Bird Electronics) mounted with 8L externally
156 sprung Niskin bottles (Ocean Test Equipment). The rosette was deployed on Spectra line using a
157 metal-free block. All samples were processed in a HEPA-filtered, positive pressure trace metal
158 clean 'bubble' within a laboratory van. Bottles were filtered with Acro-Pak 1500 cartridge filter
159 (0.8 and 0.2 μm pore size) into 1 L and 4 L LDPE bottles (Nalgene). All plasticware was
160 rigorously cleaned by soaking in 2% Citranox overnight, followed by 1 week in a 10%
161 hydrochloric acid (HCl) bath and extensive rinsing with ultra-high purity water.

162 After returning to the laboratory, samples were acidified to pH 1.8 with 1 mL L^{-1} distilled
163 HCl for several months. 15 mL aliquots were spiked with an isotope solution containing ^{57}Fe,

^{58}Fe, ^{62}Ni, ^{65}Cu, ^{110}Cd, and ^{111}Cd, extracted with Nobias PA-1 resin via a sea-FAST preconcentration system (Elemental Scientific), and eluted in 3 M nitric acid with a 1 ppb Indium internal standard. Concentrations of Fe, Mn, Ni, Cu, and Cd were analyzed by Element 2 Inductively Coupled Plasma Mass Spectrometry (ICP-MS, Thermo Scientific) as previously described (Hawco et al., 2020). Preconcentration blanks (0.093 ± 0.015 nM Fe, n = 29) were subtracted from measured values. The accuracy of these measurements was confirmed by analysis of GEOTRACES community reference seawater samples GS (0.55 ± 0.01 nM Fe, n = 3) and GSP (0.19 ± 0.03 nM Fe, n= 3), which agree with current consensus values (GS: 0.546 ± 0.046 nM, GSP: 0.155 ± 0.045 nM, www.geotraces.org/standards-and-reference-materials).

2.4 Siderophore analysis by HPLC-ICPMS and HPLC-MS/MS

Iron-binding ligands and siderophores were extracted from 4 L of 0.2 μm filtered seawater onto solid phase extraction columns at a flow rate of 20 mL min^{-1}. Prior to extraction, 6 mL Bond-Elut ENV columns (1 g, Agilent) were activated by passing 9 mL of high-purity methanol (Fisher Optima), 3 mL of 10 mM HCl, and 6 mL ultra-high purity water. Samples were then rinsed with 6 mL water, frozen at -20 ºC, and returned to the laboratory at Woods Hole for processing. Immediately prior to analysis, columns were thawed and ligands were eluted with 12 mL methanol. Extracts were concentrated at 35 °C to ~1.5 mL using a SpeedVac (Thermo Scientific). Aliquots were evaporated to dryness, and reconstituted in ultra-high purity water.

Iron ligands were analyzed using a Dionex Ultimate 3000 bioinert liquid chromatography system (Thermo Scientific) fitted with a C18 column (0.5 mm x 150 mm, 5 μm, Agilent). Compounds were eluted at a flow rate of 40 μL min^{-1} with a 20 min gradient from 5 to 90% solvent B, followed by a 10 min gradient from 90% to 95% solvent B, and a 5 min isocratic hold at 95% solvent B (solvent A: 5 mM aqueous ammonium formate, solvent B: 5 mM methanolic

ammonium formate). Eluent was plumbed directly into a quadrupole ICP-MS (iCAP-Q, Thermo Scientific), using instrument settings described in Bundy et al. (2018). Instrument sensitivity was determined with 4-point calibration curve of ferrichrome and ferrioxamine E standards. To identify siderophores, the liquid chromatography system was coupled to an Orbitrap Fusion mass spectrometer (Thermo Scientific) equipped with a heated electrospray ionization (H-ESI) source. Tentative identifications are made by comparison to known siderophore masses and retention times, as well as the presence of iron isotope pattern for siderophores bound to ^{54}Fe and ^{56}Fe. Ultra-high purity solvents and reagents were used throughout. Expanded details of this protocol are described in Boiteau and Repeta (2015).

2.5 Fe amendment incubations

Fe limitation of primary production was investigated with multi-day incubations conducted at *in situ* light and temperature conditions on a surface-tethered array. Seawater was collected from nighttime trace metal rosette casts and subsampled into cleaned 30 mL, 500 mL and 2 L polycarbonate bottles (Nalgene). For Fe amended treatments (+Fe), 2 nM Fe was added directly to incubation bottles (as 5 μM $FeCl_3$ in a 10 mM HCl solution). At the DCM, additional treatments were also conducted using Fe bound to amphibactin siderophores purified by HPLC from cultures of *Vibrio cyclitrophicus* 1F-53 following Boiteau et al. (2016) and commercially available ferrioxamine B (Sigma). Siderophore-Fe complexes were added to final concentrations of 2 nM Fe with stock solutions stored at 4 ºC until use. 500 mL bottles and 2 L bottles were mounted on the array with custom-built acrylic frames and 30 mL bottles were placed in mesh bags and affixed to the array line. Dark incubations were conducted in vinyl dry-bags with pin-holes cut to allow exchange with surrounding waters with minimal light penetration. All processing was performed in the trace metal free bubble underneath HEPA-filtered workstations.

Bottles were stored in coolers prior to deployment to minimize light and temperature perturbations during set up.

The arrays were deployed before sunrise and allowed to drift freely for 64 hr, when they were recovered (after sunset). At this point, 500 mL bottles were spiked with ^{14}C bicarbonate and 30 mL bottles were spiked with ^{3}H-leucine, prepared as described previously (Viviani & Church, 2017). Both radioisotope solutions were cleaned of metals using Chelex-100 resin (Bio-Rad; prepared according to Sunda et al., 2005) conditioned with unlabeled bicarbonate and leucine solutions at equal concentration. 500 mL and 30 mL bottles were then re-affixed to the array, which was deployed prior to sunrise, approximately 72 hr after the start of the experiment. Incubations to measure primary and bacterial production continued until sunset (~88 hr) where the arrays were recovered and measured according to established protocols (Viviani & Church, 2017). 2 L bottles were harvested after initial recovery of the array (at 64 hr), filtered onto 25 mm 0.2 μm polyethersulfone filters, and preserved with RNA-later and frozen at -80 °C. 16S rRNA genes were amplified from extracted genomic DNA with primers targeting the V4-V5 hypervariable regions and sequenced on an Illumina MiSeQ. Amplicon sequence variants were generated in DADA2 (Callahan et al. 2016). Full description is provided in the supporting information.

Following the deployment of the *in situ* array, additional seawater from the DCM was collected in 2 L bottles and incubated on deck in incubators (Caron) with light and temperature set to conditions matching the DCM in each eddy. Filtered control experiments were conducted in parallel and samples for HPLC-ICPMS analyses were collected after 5 days of incubation.

231 *2.6 Transcriptome searches*

232 Metatranscriptome samples were collected at ~4 hr intervals for three days from
233 isopycnal surfaces within the DCM during the Lagrangian sampling of the cyclonic (25.24 kg m^{-3})
234 and anticyclonic eddies (24.43 kg m^{-3}; n = 18 for each eddy). Procedures for filtration,
235 preservation, addition of quantitative standards, sequencing and assembly followed published
236 protocols (Gifford et al., 2016; Wilson et al., 2017) and are described fully in the supporting
237 information. *Prochlorococcus* iron responsive genes were identified from the culture
238 experiments of Thompson et al. (2011). The abundance of gene transcripts (as copies mL^{-1}) were
239 aggregated at the genus level and then normalized to total *Prochlorococcus* transcripts.The
240 statistical significance of the relative change in expression was tested using a Kruskal-Wallis test
241 in SciPy Python package (Virtanen et al., 2020).

242 *2.7 Analysis of Hawaii Ocean Time-series datasets*

243 Hawaii Ocean Time-series data from Station ALOHA were accessed using the Hawaii
244 Ocean Time-series data organization and graphical system (HOT-DOGS:
245 hahana.soest.hawaii.edu/hot/hot-dogs/), except for dFe data, which are replotted from
246 Fitzsimmons et al. (2015). Direct comparisons to the MESO-SCOPE expedition are restricted to
247 May – September months, while comparisons with PAR are conducted with monthly averages
248 throughout the year (Karl et al., 2021). Monthly mean PAR values at specific depths are
249 calculated as the product of the monthly averages of daily-integrated irradiance at the ocean
250 surface and the fraction of surface PAR at ‘standard’ HOT depths.

251

3 Results and Discussion

3.1 Mesoscale eddies as natural iron fertilization experiments to the lower euphotic zone: concepts and predictions

Mesoscale eddies form from instabilities in large scale currents and can isolate waters for several months while transporting them hundreds of kilometers from their origin (Chelton et al., 2011; Zhang et al., 2014). The rotation of mesoscale eddies leaves a characteristic distortion in the corrected sea-level anomaly (SLA_{corr}; see Barone et al., submitted). Anticyclonic motions are associated with SLA maxima and accumulation of surface waters. Conversely, cyclonic eddies are associated with SLA minima and a depletion of surface water near the eddy center. Although there are myriad perturbations that can be encouraged by eddy activity (McGillicuddy Jr, 2016), the most consistent feature of mesoscale eddies is the vertical displacement of density strata according to eddy polarity: cyclonic eddies lift denser waters upward, while anticyclonic eddies depress isopycnal surfaces downward (Barone et al., 2019; Siegel et al., 1999; Wunsch, 1997).

Mesoscale perturbation is of special relevance to the lower euphotic zone, where eddies alter the balance between light (largely a function of depth) and nutrient concentration (a function of density) that influence phytoplankton growth in the DCM (Figure 1). Uplift of denser, nutrient-rich waters associated with cyclonic eddies can increase NO_3^- supply relative to a given light intensity (isolume), while anticyclones displace the nutricline downward, decoupling DCM isolumes from the diffusive supply of nitrate from below.

The effect of mesoscale perturbation can be separated into two conceptual stages: 1) the initial, physical perturbation, and 2) the biological response to the physical perturbation. For the case of the cyclonic eddy, isopycnal uplift will shift the original DCM layer to shallower depths, where light absorption does not require the same degree of photo-acclimation. Over time, the

original DCM is expected to fade while a new DCM layer emerges underneath, near the 0.5 mol photon m^{-2} day^{-1} optimum that supported the DCM prior to perturbation (Letelier et al., 2004). For the anticyclone, the original DCM will be positioned too deeply for photosynthesis to remain viable, leading to the development of a new DCM in shallower waters that approach the 0.5 mol photon m^{-2} day^{-1} isolume.

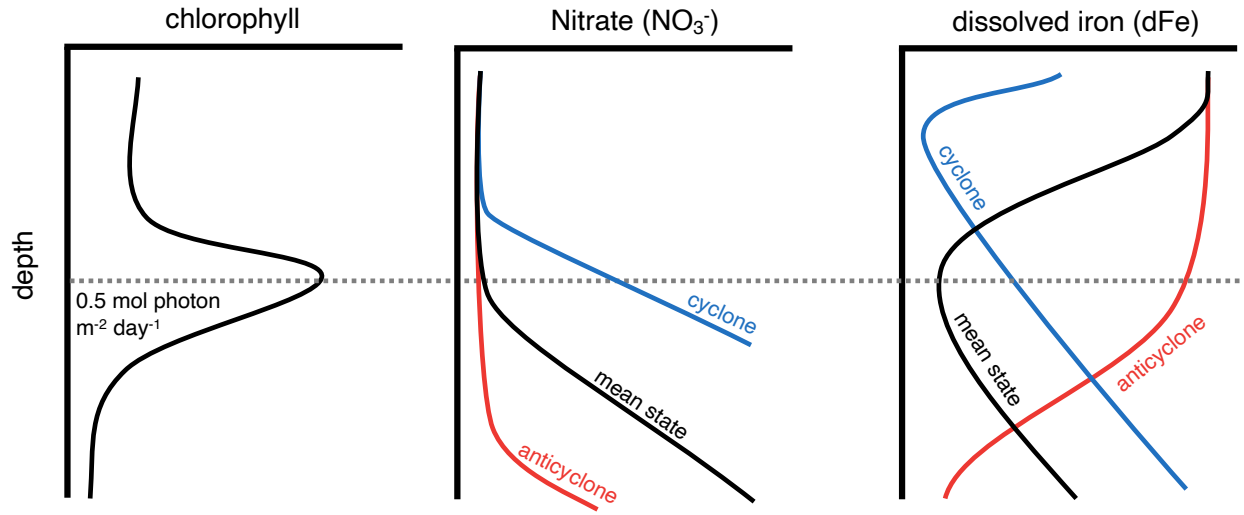

Figure 1. Idealized distributions of chlorophyll, nitrate, and dissolved iron in the North Pacific subtropical gyre (mean state, black lines). The deep chlorophyll maximum (DCM) is positioned close to the 0.5 mol photon m^{-2} day^{-1} isolume. Perturbations to the lower euphotic zone are induced by cyclonic (blue) and anticyclonic eddies (red). Downward motions in the anticyclone result in greater dFe concentrations at the DCM isolume while cyclonic eddies increase both dFe and nitrate.

Because the original DCM overlaps with a minimum in dFe, with concentrations increasing both above and below, regrowth of the DCM within a mesoscale eddy will occur in waters wth higher dFe (Fig. 1). The cyclonic eddy DCM will regrow in an environment that now hosts higher dFe from the nutricline, in addition to higher NO_3^-. In contrast, an anticyclone DCM will regrow within lower density waters, containing elevated dFe originating from the surface but

with potentially lower NO_3^-. Thus, for eddies that are sufficiently long-lived, re-equilibration of the lower euphotic zone ecosystem will occur in distinct nutrient regimes: the centers of anticyclones resemble an Fe addition without NO_3^-, while cyclones represent a simultaneous addition of Fe and NO_3^- (Fig. 1). From this, we hypothesize that both eddy types would relieve iron limitation at the DCM, if it occurred, and would increase primary production and carbon export relative to baseline values at similar isolumes. In contrast, prevalence of nitrogen limitation would favor a productivity increase within cyclonic eddies only. The ecosystem response to mesoscale forcing may therefore reveal the extent of iron limitation at the DCM in the mean state.

3.2 Iron, nutrient and phytoplankton perturbations along an eddy dipole

During July 2017, we examined the biogeochemistry of a cyclonic-anticyclonic eddy pair in the central North Pacific Subtropical Gyre (Figure 2). A more detailed description of the 2017 MESO-SCOPE expedition is presented by Barone et al. (submitted). Satellite tracking of both eddies suggested a similar point of origin northeast of Hawai‘i, with estimated ages of 100 days for the cyclonic eddy and 140 days for the anticyclone. At the time of their sampling, these eddies were near their peak SLA: +24 and –15 cm for the anticyclone and cyclone, respectively (Fig. 2a). Eddy centers were associated with large perturbations to the density structure of the upper ocean, with an eddy-to-eddy difference of ~120 m for the depth of the 25.0 kg m^{-3} isopycnal (σ_θ), which falls within the nitracline at Station ALOHA (1.9 ± 0.9 μM NO_3^-, 190 m mean depth; Fig. 2b). In contrast, the position of the DCM between eddy centers varied by less than 20 m, corresponding to 25.2 kg m^{-3} in the cyclonic eddy (104 m depth) and 24.4 kg m^{-3} in the anticyclone (118 m). Multi-day integrals of PAR indicated that the DCM of both eddies occurred at a similar light flux: 0.46 ± 0.18 and 0.29 ± 0.02 mol photon m^{-2} day^{-1} for the cyclonic

and anticyclonic eddies, respectively (Table 1). While these irradiance estimates fall slightly below the canonical value of 0.5 mol photon m^{-2} day^{-1} (Letelier et al., 2004), they suggest that the eddies sampled in 2017 were sufficiently mature and stable to allow for biological re-equilibration of the lower euphotic zone to an optimal irradiance.

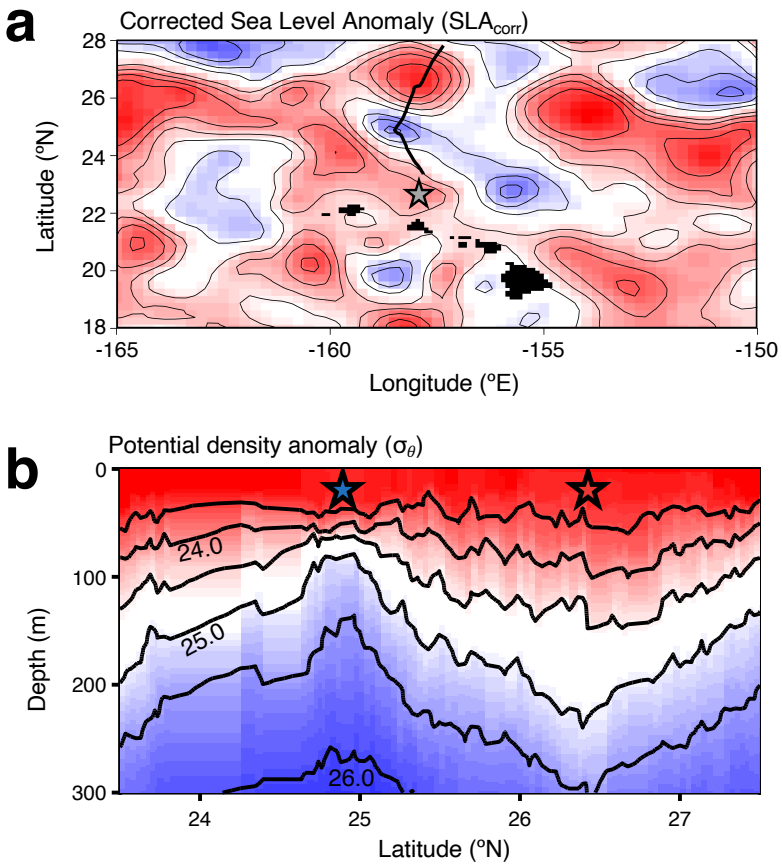

Figure 2. Characterization of an eddy dipole in the North Pacific Subtropical gyre during July 2017. a) Corrected sea-level anomalies (SLA_{corr}) across the region. Blue shading highlights minima in SLA_{corr}, marking cyclonic eddies, while SLA_{corr} maxima (red) coincide with anticyclones. Contours mark 5 cm intervals, excluding 0 cm (white shading). b) A section of potential density anomaly (σ_θ) following the bolded line of the cruise track in Fig. 2a. Uplift of dense isopycnal surfaces (blue shading) peaks at 24.9 °N and depression of surface water masses (red shading) is greatest at 26.4 °N. Blue and red stars indicate stations occupied for hydrographic sampling in the cyclonic and anticyclonic eddy centers, respectively. The gray star in Fig. 2a indicates the location of Station ALOHA.

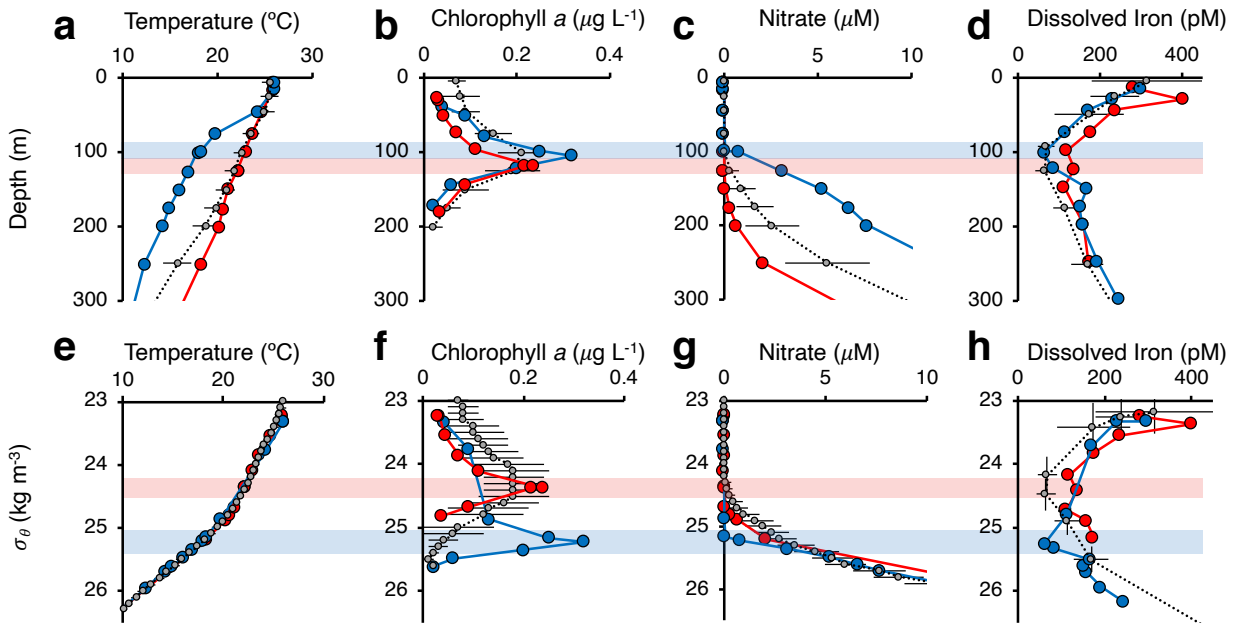

Figure 3. Perturbation of water column properties in cyclonic (blue lines) and anticyclonic (red lines) eddy centers as a function of depth (a–d) and potential density anomaly (σ_θ; e–h). Long term averages for May–September observations from Station ALOHA, located nearby, are plotted in gray. Decoupled depth profiles of temperature (a) collapse when plotted against density (e). The deep chlorophyll maximum (DCM) occurs at a similar depth (b) in both eddies but on distinct density surfaces (f) and coincides with removal of nitrate (c, g) and dissolved Fe (d, h) at the cyclonic eddy DCM. The DCM of each eddy is marked in all panels by red and blue shading.

The ecosystem response to eddy-driven perturbation left clear signatures in nutrient inventories. At 200 m depth (below the photosynthetic compensation irradiance), isopycnal uplift in the cyclonic eddy led to NO_3^- concentrations of 7.65 μM, an order of magnitude greater than observed in the anticyclonic eddy at the same depth (0.69 μM; Figure 3). Most of this difference in NO_3^- could be accounted for solely by the vertical displacement of water masses. As a result, variability decreased substantially when eddy center profiles were compared against density (Fig. 3). Similar depth offsets were observed for profiles of dissolved Ni, Cu, and Cd, and Mn, which

also re-aligned when plotted against density (Fig. S1). However, between 25.0-25.3 kg m^{-3}, the cyclonic eddy contained 1-3 μM less NO_3^- than the anticyclonic eddy. This density range overlapped with a large population of small eukaryotic phytoplankton (picoeukaryotes; 5 x 10^3 cells ml^{-1}) in the cyclonic eddy DCM (Figure 4). Together, these observations suggest that uplift of nutrient rich waters into the lower euphotic zone enabled significant biological uptake of NO_3^- in the cyclonic eddy, consistent with the predictions of the conceptual model.

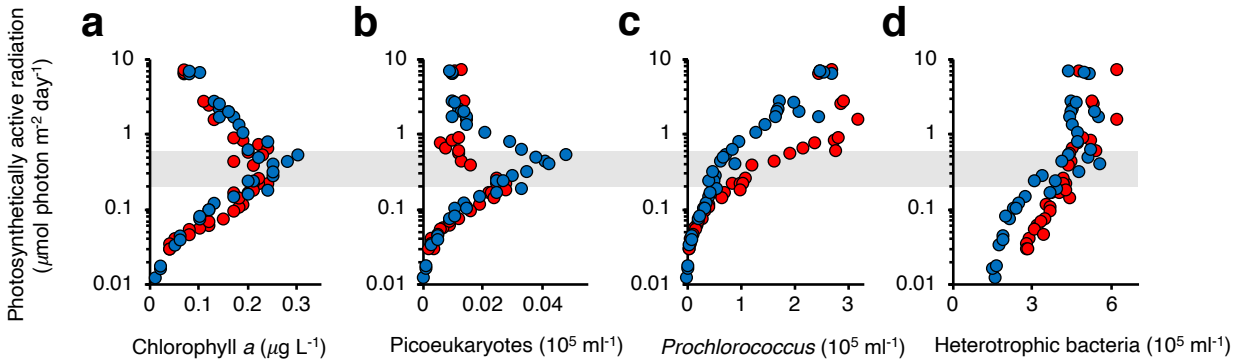

Figure 4. Alignment of chlorophyll *a* (a), picoeukaryotes (b), *Prochlorococcus* (c), and heterotrophic bacteria (d) by ambient light (as photosynthetically active radiation, PAR) in the cyclonic (blue) and anticyclonic (red) eddies. The grey shading highlights the range in PAR associated with the DCM in both eddies (0.2–0.6 μmol photon m^{-2} d^{-1}), which also encompasses the DCM at Station ALOHA.

In contrast, the depth profile of dFe in the cyclonic eddy resembled profiles in the anticyclonic eddy and under non-eddy conditions at Station ALOHA. Each of these profiles contained a minimum at the DCM (Fig. 3d), despite the fact that the DCM of the cyclonic eddy occurred on a distinct isopycnal surface that is usually associated with elevated Fe from remineralization (Fig. 3h). Indeed, dFe at 25.25 kg m^{-3} – within the DCM of the cyclonic eddy – was 63 pM, compared to 170 pM in the anticyclone at a similar density (25.15 kg m^{-3}, 250 m depth). The latter value is similar to an average dFe of 152 ± 46 pM between 175-250 m depth at

Station ALOHA (Fitzsimmons et al., 2015), corresponding to a range of σ_θ between 24.9-25.5 kg m^{-3}. Thus, NO_3^- uptake in the cyclonic eddy coincided with dFe uptake on the order of 100 pM. While the anticyclone also had a minimum in dFe at the DCM, this concentration (~136 pM) was roughly double the dFe measured in both the cyclone and at Station ALOHA (Table 1), likely reflecting downwelling of dFe from surface waters.

3.3 Direct tests of Fe limitation in the lower euphotic zone

To determine the influence of the eddy perturbation on ecosystem productivity, primary production was measured during a period of Lagrangian sampling in the centers of both eddies (Fig. 5). Consistent with isopycnal evidence for uptake of NO_3^- and dFe, rates of primary production in the DCM (by the ^{14}C method) were moderately higher (0.21 ± 0.03 μM C day^{-1} between an irradiance of 0.2 – 0.6 mol photon m^{-2} day^{-1}, n = 4) compared to rates at equivalent PAR in the anticyclonic eddy (0.10 ± 0.01, n = 2) or average values from Station ALOHA (0.12 ± 0.04 μM C day^{-1}, Table 1). This amounts to a doubling of productivity within the DCM, but the effect is small compared to the large increase in ^{14}C uptake at all sites with increasing light (Fig. 5). Similar relationships between irradiance and primary production in the anticyclone and at ALOHA suggest that the two-fold increase in dFe at the anticyclonic eddy DCM did not stimulate primary production.

Longer term incubations were conducted to evaluate the sensitivity of primary production to dFe. After 3 days of incubation *in situ*, unamended control incubations in the cyclonic eddy harbored an unusual maximum in ^{14}C uptake at 100 m depth, just above the DCM, equal to 0.43 ± 0.04 μM C day^{-1} (mean ± 1 standard deviation of 3 bottle replicates; Fig. 6). This rate is more than 3 standard deviations above mean May–September primary production at 100 m for Station ALOHA (0.21 ± 0.07 μM C day^{-1}), and nearly equal to the maximum rate of 0.55 μM C day^{-1}

over the entire record at 100 m (n = 121). Iron addition to this depth increased primary production slightly to 0.54 ± 0.08 μM C day^{-1}, but not significantly ($p > 0.05$, Student's t-test). At the DCM of the cyclonic eddy (incubated at 110 m), primary production was lower: 0.25 ± 0.05 μM C day^{-1} in the control and 0.27 ± 0.07 μM C day^{-1} in the 2 nM Fe treatment. Equivalent primary production was also observed in control and +Fe treatments throughout the lower euphotic zone of the anticyclone (Fig. 6). Additions of Fe as Fe-amphibactin D or ferrioxamine B siderophores also did not increase DCM primary production relative to the unamended control in either eddy center (Fig. S2).

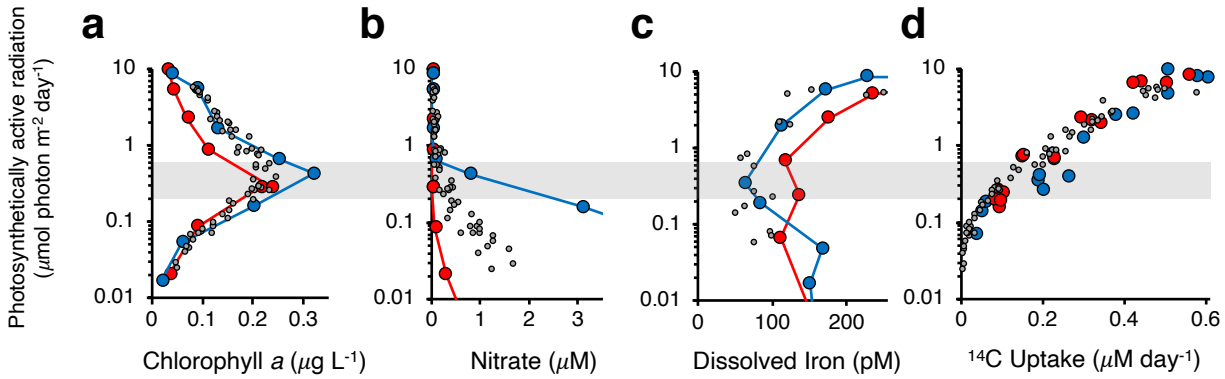

Figure 5. Intercomparison of nutrients, iron, productivity and light. Cyclonic (blue) and anticyclonic (red) eddy center profiles of (a) chlorophyll *a*, (b) nitrate, (c) dissolved iron from Fig. 3, and (d) rates of ^{14}C uptake from three separate 12-hour incubations at *in situ* temperature and light during the Lagrangian period. Each circle for ^{14}C uptake represents the mean of triplicate incubations. Monthly averaged data from HOT are plotted as grey circles. Note that these 12-hour primary production measurements are distinct from the multi-day experiments in Figure 6.

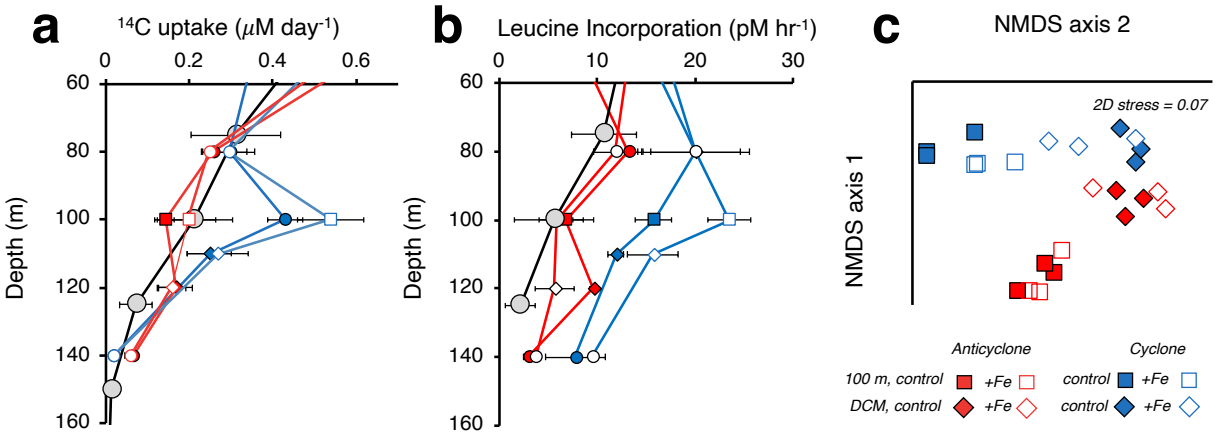

Figure 6. Tests of iron limitation in the cyclone (blue) and anticyclone (red) centers. Following 3 days of incubation at *in situ* light and temperature, 12-hour ^{14}C uptake (a) and leucine incorporation (b) assays were conducted for unamended seawater (filled symbols) and 2 nM Fe additions (open symbols). Experiments at 100 m (squares) and the DCM (diamonds) of the cyclonic eddy show a significant response for leucine incorporation in +Fe experiments relative to controls. Grey cirlces show May – September values from Station ALOHA. c) Non-metric multi-dimensional scaling (NMDS) ordination of 16S rRNA gene amplicon sequences from *in situ* incubations indicate distinct communities in each eddy and at each depth, but limited change due to Fe addition. NMDS based on weighted UniFrac distance matrix of amplicon sequence variants.

Although primary production did not change significantly following iron addition, Fe did increase rates of ^{3}H-leucine incorporation at both 100 m and 110 m in the cyclonic eddy. At 100 m, leucine incorporation under ambient light increased from 15.7 ± 1.8 pM hr^{-1} (control) to 23.5 ± 2.2 pM hr^{-1} (+Fe; $p < 0.05$, Student's t-test; Fig. 6b). A considerably smaller increase was observed in dark incubations at this depth (13.3 ± 1.2 vs. 15.4 ± 0.08, Fig. S2). At the DCM (110 m), Fe also increased rates of ^{3}H-leucine incorporation ~30% above unamended controls under ambient light. Analysis of the bacterial community at 100 m and 110 m by amplification and

sequencing of 16S rRNA genes indicated dominance of *Prochlorococcus* and *Pelagibacter*, but community composition in ambient light incubations did not differ significantly between controls and +Fe treatments (Fig. 6c). In the anticyclone, rates of ^{3}H-leucine incorporation were similar to observations at Station ALOHA (n = 114; Viviani & Church, 2017), and lower throughout the water column compared to the cyclonic eddy. Leucine incorporation was not stimulated with Fe addition at 100 m, nor at the DCM (120 m), consistent with greater dFe in the anticyclonic eddy ($p > 0.05$, one way ANOVA). Despite distinct prokaryotic communities between eddies and between 100 m and the DCM (Fig. 6c), no significant changes in community structure (based on rRNA gene analysis) were observed following Fe addition in the anticyclone.

3.4 Meoscale perturbation of siderophore distributions and cycling

Most dFe in the upper ocean is strongly bound to organic ligands, including siderophores, which cycle at an unknown rate. Prior measurements of excess Fe ligand concentrations in the North Pacific Subtropical Gyre appear invariant over the upper 300 m (Fitzsimmons et al., 2015), but siderophores with unique depth distributions have been identified throughout the water column at Station ALOHA (Bundy et al., 2018). In the eddy dipole, HPLC-ICPMS analyses highlighted significant shifts in Fe speciation between eddies. Both eddies displayed an unresolved complex mixture of Fe ligands that appear as a hump in the chromatogram baseline (Fig. 7a). Within each eddy, these unresolved ligands were roughly constant with depth but were greater in the anticyclone (44 ± 5 pM) compared to the cyclone (17 ± 2 pM). Identified ligands in the anticyclone included the high-affinity and polar siderophore ferrioxamine-E and a suite of amphibactins, which are non-polar and have weaker binding affinity for Fe (Bundy et al., 2018). In the cyclonic eddy, ferrioxamine-E was the most abundant siderophore but total siderophores averaged from 0–150 m were much lower (0.3 pM) compared to the anticyclonic eddy (2.6 pM).

Indeed, siderophore concentrations in the cyclonic eddy DCM (0.13 pM) were 15-fold lower than at a corresponding density in the anticyclone (2.0 pM at 250 m), perhaps reflecting uptake of these compounds following uplift into the euphotic zone (Fig. 7a). The differences in dFe and siderophore abundances in the cyclonic and anticyclonic eddies suggest that their turnover times in the upper ocean are fast relative to the lifetimes of these eddies.

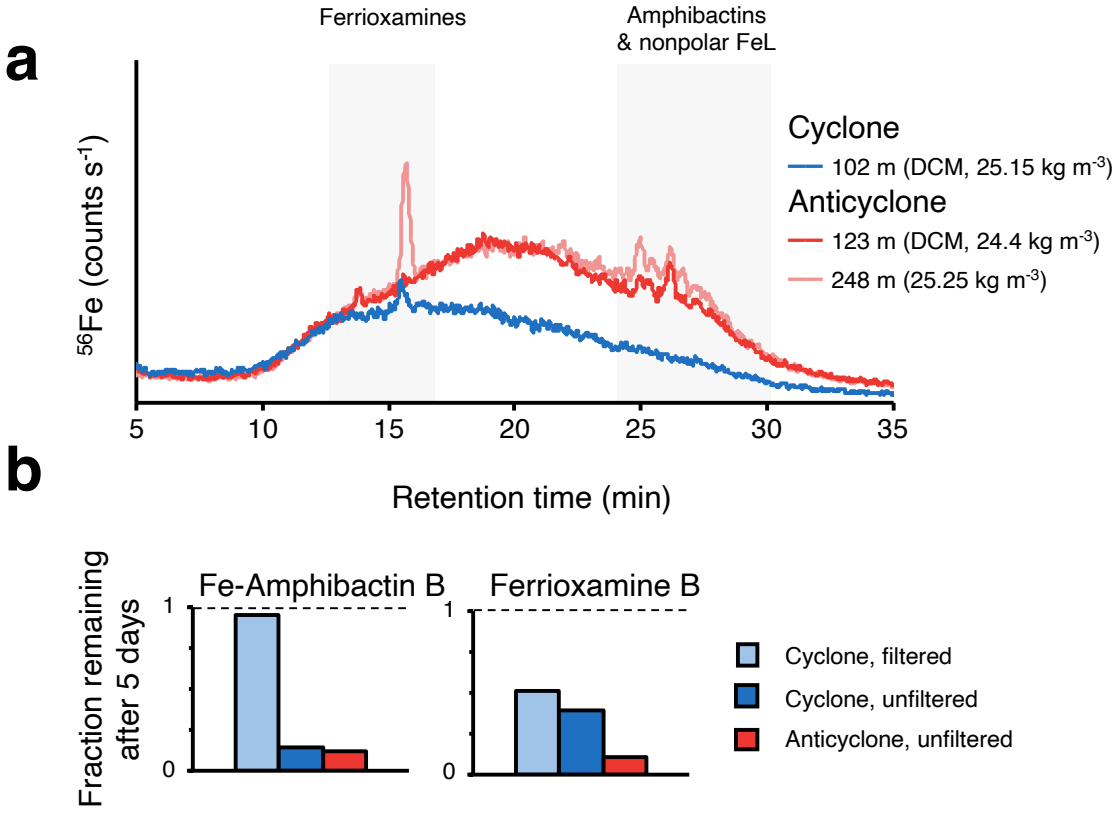

Figure 7. a) HPLC-ICPMS chromatograms of Fe-binding ligands in the DCM of the cyclonic and anticyclonic eddies (blue and red lines, respectively), and from 250 m in the anticyclonic eddy (pink line). The 250 m anticyclone sample corresponds to a similar density as the cyclonic eddy DCM. Early elution of ferrioxamines (ca. 15 min) is highlighted in comparison to later elution (25–30 min) of amphibactins and other non-polar siderophores. b) On-deck incubation experiments showing loss of Fe-amphibactin D or Ferrioxamine B added to DCM waters from the cyclonic eddy (blue bars) and anticyclonic eddy (red bars) after 5 days of incubation. Filtered control experiments (light blue bars) were only conducted in the cyclonic eddy, and suggest significant abiotic loss of ferrioxamine B but not Fe-amphibactin D.

To estimate the rate of siderophore cycling, parallel incubations were also performed on-deck, with 2 nM ferrioxamine B and Fe-amphibactin D added to DCM waters from both eddies. After 5 days of incubation at similar light and temperature, concentrations of ferrioxamine B and Fe-amphibactin D in waters from the cyclone DCM decreased by 61 % and 86 %, respectively (Figure 7b). However, ferrioxamine B added to a 0.2 μm filtered control experiment also decreased by 49 %, indicating that part of the loss in the unfiltered experiments was due to abiotic factors (e.g. hydrolysis, chelate dissociation). In contrast, 95 % of added Fe-amphibactin D was recovered in the filtered controls, indicating that its removal from unfiltered incubations was primarily due to biological activity. Similar levels of amphibactin D removal (88 %) were also found in the anticyclonic eddy, where greater ferrioxamine B removal was observed (90 %). These experiments provide evidence that amphibactins represent a readily bioavailable Fe source to the microbial community, which is consistent with the uptake inferred in the cyclonic eddy DCM based on isopycnal comparisons (Fig. 7a). Yet, amphibactins may not be bioavailable to the entire microbial community: addition of 2 nM Fe-amphibactin D did not increase ^{3}H-leucine incorporation in the cyclonic eddy DCM, despite the increase observed with addition of unchelated Fe (Fig. S2). Overall, there is a need to constrain the bioavailability and turnover times of these siderophores, especially the roles of heterotrophic uptake and abiotic degradation that could limit their longevity below the euphotic zone.

3.5 Prochlorococcus Fe limitation in the cyclonic eddy?

The physical perturbation of the anticyclonic eddy can be conceptualized as an Fe fertilization to the DCM (Fig. 1). By the time this eddy was sampled, the DCM had repositioned near the 0.5 mol photon m^{-2} day^{-1} isolume, with residual dFe concentrations that were significantly greater than observed at Station ALOHA (Figs. 3, 5). Yet, this apparent increase in

dFe was not matched by increased primary productivity (by ^{14}C uptake) or ^{3}H-leucine incorporation relative to measurements at Station ALOHA (Figs. 5, 6). Additional evidence for a significant biological response in the lower euphotic zone (e.g. O_2 accumulation or increases in sinking organic matter flux) is also lacking in this eddy (Barone et al., Submitted). The simplest explanation for these observations is the absence of a bioavailable nitrogen source that would allow biomass and/or productivity to increase beyond typical values, but this implies that any effect of iron on DCM productivity first requires an adequate N supply, likely ruling out proximal Fe-limitation under non-eddy conditions.

Simultaneous N and Fe inputs did occur in the center of the cyclonic eddy, which hosted increased primary production near the DCM. Increased nutrient delivery to DCM isolumes is consistent with the emergence of picoeukaryotes, which can grow rapidly with a NO_3^- source, and the decline of *Prochlorococcus* (Fig. 4), often considered to grow solely on reduced N sources (e.g. ammonia, urea, and amino acids, (Moore et al., 2002)). Despite this conception, genomic analyses have found that genes for nitrate reductase are widespread in LL1 *Prochlorococcus* ecotypes, whose abundance peaks near the DCM at Station ALOHA (Berube et al., 2016, 2019; Casey et al., 2007; Malmstrom et al., 2010). Thus, increased NO_3^- supply may still allow an increase in *Prochlorococcus* biomass.

Relatively high iron requirements for *Prochlorococcus* photosynthesis may make them less competitive when NO_3^- supply increases. Experiments at DCM conditions with a low-light adapted *Prochlorococcus* (MIT1214 strain, LL1 ecotype) have indicated that the onset of Fe limitation is associated with an Fe:C ratio of 30–40 μmol:mol (Hawco, et al., 2021), which is similar to the HLI *Prochlorococcus* strain MED4 when grown under low light (~45 μmol:mol; Cunningham & John, 2017; Shire & Kustka, 2015). In the center of the cyclonic eddy, removal

of 100 pM dFe was associated with the uptake of 2 μM NO_3^-. Assuming a C:N ratio of 6.6, the corresponding Fe:C ratio, 8 μmol:mol, is below these *Prochlorococcus* Fe:C thresholds, suggesting that NO_3-dependent growth in the cyclonic eddy would lead to Fe limitation. In contrast, some eukaryotic phytoplankton can grow at low irradiance with an Fe:C below 5 μmol:mol (Maldonado & Price, 1996; Marchetti et al., 2006; Strzepek et al., 2012), which could allow NO_3^- drawdown without Fe limitation. While this reasoning applies mostly to the intensification stage of the cyclonic eddy where heightened export occurred (taking place prior to our observations; Barone et al., submitted), persistent and steep NO_3 gradients imply that diffusive mixing maintained a similar Fe:NO_3 supply ratio during the mature phase of this eddy (~7.6 μmol Fe: mol C when converted with a 6.6 C:N ratio; see Table 1).

The primary evidence for Fe stress within the cyclonic eddy comes from greater leucine incorporation when iron was added to multi-day incubations, especially in bottles receiving ambient light. At Station ALOHA, much of the leucine uptake and incorporation under sunlit conditions is conducted by *Prochlorococcus*, including cells in the lower euphotic zone (Björkman et al., 2015; Church et al., 2006). Therefore, the Fe stimulation of leucine incorporation may reflect enhancement of *Prochlorococcus* activity that was not apparent (or statistically resolvable) in bulk ^{14}C uptake. At 100 m, the relative Fe stimulation effect was much greater in the light (~50%) than the dark (16%), consistent with *Prochlorococcus*-driven incorporation. Because NO_3^- uptake and reduction via the nitrate reductase enzyme is expected to increase Fe requirements (Raven, 1988), *Prochlorococcus* leucine incoproration may be motivated by acquisition of reduced nitrogen rather than organic carbon (Duhamel et al., 2018). Stimulation of *Prochlorococcus* metabolism is also consistent with their abundance in these incubations: 16S rRNA gene amplicon sequencing of +Fe and control treatments did not provide

evidence for emergence of a new population of possibly Fe-limited heterotrophic bacteria (Fig. 6c), suggesting that the leucine incorporation signal is driven by a population that was already dominant (e.g. *Pelagibacter*, *Prochlorococcus*).

However, there are also potenitial experimental artifacts for the multi-day incubations that can complicate comparisons to the surrounding seawater. At a fixed depth, these incubations provide an incomplete representation of the dynamic light fields caused by inertial waves and other physical processes, which result in vertical oscillations with periods of hours to days (Letelier et al., 1993). Bottled phytoplankton are also isolated from numerically rare and vertically-migrating grazers. Relief from grazing pressure over several days could support increases in autotrophic biomass and explain why the large productivity maximum at 100 m in the multi-day incubations was not found in multiple 12-hour ^{14}C productivity measurements in the same eddy. We speculate that if isolation from protistan grazers and zooplankton allowed the biomass of some phytoplankton to increase, it would also have reduced the recycling of biomass Fe needed to sustain the growth of *Prochlorococcus*, enabling the observed Fe stimulation of leucine incorporation.

Indeed, we were unable to find strong evidence for *Prochlorococcus* Fe stress under background conditions. Like other phytoplankton, the onset of Fe limitation in *Prochlorococcus* in culture is associated with a decrease in the Chl:C ratio (Hawco et al., 2021; Sunda & Huntsman, 1997). In both eddies, there is a similar relationship between PAR and derived *Prochlorococcus* Chl:C, calculated as the sum of divinyl chlorophyll *a* and *b*, which are both specific to *Prochlorococcus*, using a uniform mol C cell^{-1} conversion (Figure 8). This comparison indicates that *Prochlorococcus* photo-acclimation is not strongly impacted by the low dFe in the cyclonic eddy. We also searched for known Fe stress markers from transcriptomes

551 sampled in the DCM throughout the Lagrangian observation period. Iron limitation is expected
552 to up-regulate expression of *isiB*, which encodes the electron carrier flavodoxin that substitutes
553 for Fe-containing ferredoxin in photosynthetic electron transport, the latter encoded by the *petF*
554 gene (Bibby et al., 2003; Thompson et al., 2011). Expression of *isiB* was slightly increased in the
555 cyclonic eddy compared to the anticyclonic eddy, while *petF* was slightly decreased (Table 2).
556 The resulting ~2-fold increase in *isiB*:*petF* ratio in the cyclonic eddy follows the direction
557 anticipated by Fe stress but falls short of the >10-fold change expected from culture studies of
558 both high and low-light adapted *Prochlorococcus* strains (Thompson et al., 2011). Similarly, the
559 small (17%) increase in expression of the *idiA* gene, encoding the periplasmic Fe binding
560 component of the iron ABC transpoter, in the cyclonic eddy matches the direction but not the
561 magnitude identified in culture (>500%). Of these genes, only *petF* (ferredoxin) met significance
562 criteria used to identify differential expression between the two eddies ($p = 0.046$, Table 2).
563 Given the muted response of these genes in the cyclonic eddy DCM, it seems possible that Fe
564 stress only emerged in *Prochlorococcus* during long-term incubations.

565 Overall, this analysis suggests that the relatively high Fe requirements of
566 *Prochlorococcus* under low irradiance may make them more sensitive to Fe limitation in the
567 DCM than eukaryotic phytoplankton, even if *Prochlorococcus* was not Fe-limited outside of the
568 multi-day incubations. It is interesting that this scenario is opposite to that outlined in the surface
569 waters of the Equatorial Pacific, where *Prochlorococcus* tend to be less vulnerable to Fe
570 limitation than eukaryotic phytoplankton (Cavender-Bares et al., 1999; Mann & Chisholm, 2000;
571 Price et al., 1994). There, the small size of *Prochlorococcus* makes them more competitive for
572 diffusive supply of recycled Fe, which may be largely unchelated (Morel et al., 2008). Bioassays
573 and molecular studies have suggested that eukaryotic phytoplankton may be able to access a

much larger portion of the dFe pool than *Prochlorococcus* (Coale et al., 2019; Kazamia et al., 2018; Lis et al., 2015; Maldonado & Price, 1999, 2001). Low irradiance near the DCM also makes Fe-chelates less prone to photodegradation or Fe photo-reduction than tropical surface waters (Barbeau et al., 2001), likely increasing reliance on specific transport mechanisms rather than uptake systems based on inorganic Fe. In the on-deck incubations under DCM conditions, added Fe amphibactin D decreased markedly after 5 days in cyclonic eddy waters (Fig. 7b), indicating that these compounds were bioavailable and that they cycle rapidly in the lower euphotic zone. It is interesting to note that similar removal was also apparent in the relatively Fe-rich anticyclone. Compared to the cyclone, the anticyclone DCM contained a similar number of heterotrophic bacteria, but fewer picoeukarytoes and more *Prochlorococcus* (Fig. 4), suggesting that the observed drawdown of siderophores may not depend on phytoplankton alone.

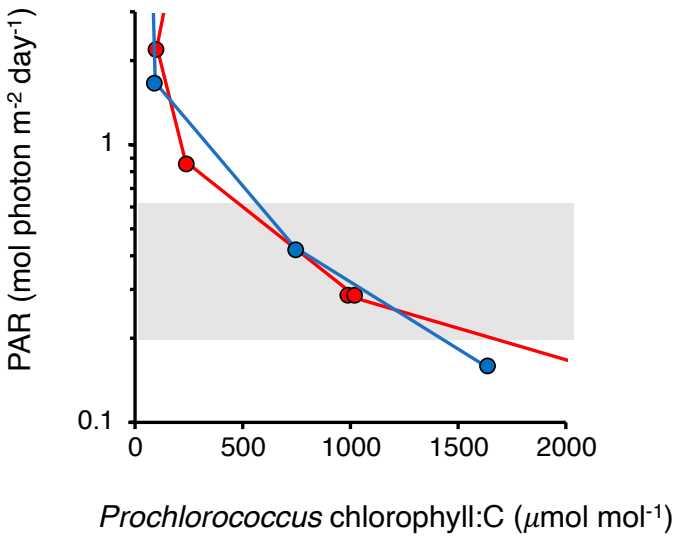

Figure 8. Estimated chlorophyll:C ratios of *Prochlorococcus* cells in the lower euphotic zone on the cyclone (blue) and anticyclone (red). Circles represent measurements conducted during the hydrographic survey, matching Figs. 3 and 5. Chlorophyll:C ratios are calculated as the sum of divinyl chlorophyll *a* and *b*, which are diagnostic of *Prochlorococcus,* with cell number converted to cell C assuming 4 fmol C per *Prochlorococcus* cell. Gray shading highlights the DCM region in both eddies as per Figs. 4 and 5.

3.6 Implications for iron limitation in the oligotrophic DCM

Taken together, these results highlight the potential for Fe stress within the microbial community in the cyclonic eddy center, which ultimately did not manifest in Fe limitation of primary production. It is noteworthy that dFe measured in the cyclonic eddy was almost identical to dFe in the lower euphotic zone at Station ALOHA (Table 1; Fitzsimmons et al., 2015). However, at similar irradiance, the cyclonic eddy supported a nearly two-fold increase in primary production relative to mean rates at Station ALOHA (Fig. 5), which increased further in the long term incubations (Fig. 6). Therefore, low dFe (50–80 pM) does not necessarily prevent increases in primary production under low light conditions.

Fe limitation of eukaryotic phytoplankton was recently reported for the DCM in the Eastern North Pacific (Hogle et al., 2018), especially close to the California coast where shoaling of isopycnal surfaces leads to greater NO_3^- supply to the lower euphotic zone (2.9–9.1 μM at the DCM), but similar dFe (0.05–0.1 nM). Other incubations at similarly high NO_3^-, but higher dFe (> 0.2 nM), have shown signs of Fe-light co-limitation, but no response to Fe addition alone (Hopkinson & Barbeau, 2008; Johnson et al., 2010). From this perspective, it is likely that the cyclonic eddy did not reach a critical rate of N supply to trigger Fe limitation for the entire phytoplankton community. Relative to eddy lifetimes on the order of 100 days or more, the short-term nature of sampling and experiments may limit this conclusion to the mature phase of these eddies. Depending on the relative kinetics of Fe and NO_3^- uptake following isopycnal uplift, more favorable conditions for Fe limitation (> 1 μM NO_3^-, < 0.1 nM dFe) may still emerge during cyclonic eddy intensification.

Compared to long term observations at Station ALOHA, however, the 2017 cyclonic eddy and anticyclonid eddies were clearly anomalous, bracketing the extremes of sea-level anomaly and the displacement of isopycnal surfaces (Barone et al., Submitted). The fact that

isopycnal shoaling and enhanced NO_3^- supply in the 2017 cyclonic eddy was insufficient to induce Fe limitation of primary production means that the possibility for Fe limitation under non-eddy conditions should be relatively narrow. Similar conclusions are reached based on retrospective analyses of the HOT program (Barone et al., 2019; Church et al., 2009). Episodes of negative sea-surface height anomaly at Station ALOHA coincide with negative isopycnal NO_3^- anomalies in the lower euphotic zone and with positive anomalies in chlorophyll, productivity and oxygen (Table S1; Barone et al., 2019). These anomalies are best explained by processes also observed in the MESO-SCOPE cyclonic eddy center in July 2017: isopycnal uplift into the euphotic zone enables primary production and NO_3^- removal. The population of picoeukaryotes also increases during these events (Barone et al., 2019). Thus, eddy-driven NO_3^- drawdown in the lower euphotic zone has been observed on several instances, suggesting that the amount of dFe that is brought into the euphotic zone is sufficient for NO_3^- uptake. Anticyclonic eddies and other episodes of positive SLA_{corr} at ALOHA also supports our observations from 2017: surface dFe injection into the lower euphotic zone following a depression of the thermocline does not lead to elevated productivity or O_2 concentration (Barone et al., 2019).

Conclusions

The pair of eddies sampled in the 2017 MESO-SCOPE project depict distinct NO_3^- and dFe supply regimes at the depths and isolumes that characterize the DCM (Fig. 5, Table 1). In the cyclonic eddy, prior removal of NO_3^- and dFe, presumably during the intensification stage, was evident in isopycnal anomlies. Low dFe:NO_3^- supply ratios from turbulent mixing also characterized the mature phase of the cyclone. The magnitude of these ratios are associated with Fe stress in *Prochlorococcus*, but may be sufficient for the picoeukaryote population found in

this eddy. Compared to Station ALOHA, atypically high primary production near the 0.5 mol photon m^{-2} day^{-1} isolume in the cyclonic eddy was supported by elevated NO_3^- but similar dFe, implying that any regulating role for iron is secondary to nitrogen and light (Fig. 5). Population control by grazers also appears to play a key role in recycling dFe to sustain this elevated productivity throughout the mature phase of these eddies. There are still key aspects of Fe budgets in the lower euphotic zone that are not constrained or considered by this work, but likely influence the ecosystem susceptibility to iron stress, especially the magnitude and labilty of particule Fe inventories, and the bioavailability of dFe. For now, we can only highlight the apparently rapid alterations of the siderophore pool as an indictator for a fast and complex iron cycle near the DCM (Fig. 7).

Meanwhile, the unusual abundance of dFe in the anticyclone DCM should have created conditions to relieve Fe-stress. In some ways, this conceptual model is consistent with elevated *Prochlorococcus* abundance in the anticyclonic eddy, and with signs of Fe stress in leucine uptake experiments in the cyclone, but not the anticyclone. However, the fact that ^{14}C primary production profiles in the anticyclone overlapped with Station ALOHA mean values implies that any Fe fertilization effect must be small in magnitude or constrained by depletion of other nutrients (e.g. nitrogen). To the extent that the biogeochemistry documented within the MESO-SCOPE eddies and at Station ALOHA represent the North Pacific Subtropical Gyre and oligotrophic regions elsewhere, our results suggest that Fe limitation is difficult to induce in the DCM. However, given its apparently higher Fe requirements, one might look for *Prochlorococcus* in the DCM as a bellwether of Fe stress that would precede the emergence of Fe limitation at the ecosystem scale.

Acknowledgments, Samples, and Data

We thank the Captain and Crew of the R/V *Kilo Moana*, Ryan Tabata, Tim Burrell, Eric Shimabukuro and all of the participants of the MESO-SCOPE expedition. Custom bottle arrays were expertly designed and constructed by Blake Watkins. The expedition and analyses were supported by the Simons Foundation SCOPE Grant 329108 to SGJ, MJC, DJR, BVM, EFD, and DMK. NJH was supported by a Simons Foundation Marine Microbial Ecology and Evolution postdoctoral fellowship (602538) and Simons Foundation grant 823167. Each of the authors certify that they have no conflicts of interest to report. Data from this manuscript can be accessed at DOI:10.5281/zenodo.5064292 and DOI:10.5281/zenodo.3750468. Amplicon sequence data can be accessed at the National Center for Biotechnology Information (NCBI) under sequence read archive PRJNA733670.

References

Achterberg, E. P., Moore, C. M., Henson, S. A., Steigenberger, S., Stohl, A., Eckhardt, S., et al. (2013). Natural iron fertilization by the Eyjafjallajökull volcanic eruption. *Geophysical Research Letters*, *40*(5), 921–926.

Barbeau, K., Rue, E. L., Bruland, K. W., & Butler, A. (2001). Photochemical cycling of iron in the surface ocean mediated by microbial iron (III)-binding ligands. *Nature*, *413*(6854), 409–413.

Barone, B., Coenen, A. R., Beckett, S. J., McGillicuddy, D. J., Weitz, J. S., & Karl, D. M. (2019). The ecological and biogeochemical state of the North Pacific Subtropical Gyre is linked to sea surface height. *Journal of Marine Research*, *77*(2), 215–245.

Barone, B., Church M. J., Dugenne M., Hawco, N.J., Jahn, O., White A. E., John S. G., Follows

M. J., Delong, E. F., & Karl, D. M. Biogeochemical dynamics in adjacent mesoscale eddies of opposite polarity. *Submitted to Global Biogeochemical Cycles.*

Becker, K. W., Harke, M. J., Mende, D. R., Muratore, D., Weitz, J. S., DeLong, E. F., et al. (2021). Combined pigment and metatranscriptomic analysis reveals highly synchronized diel patterns of phenotypic light response across domains in the open oligotrophic ocean. *The ISME Journal*, *15*(2), 520–533.

Berube, P. M., Coe, A., Roggensack, S. E., & Chisholm, S. W. (2016). Temporal dynamics of Prochlorococcus cells with the potential for nitrate assimilation in the subtropical Atlantic and Pacific oceans. *Limnology and Oceanography*, *61*(2), 482–495.

Berube, P. M., Rasmussen, A., Braakman, R., Stepanauskas, R., & Chisholm, S. W. (2019). Emergence of trait variability through the lens of nitrogen assimilation in Prochlorococcus. *Elife*, *8*, e41043.

Bibby, T. S., Mary, I., Nield, J., Partensky, F., & Barber, J. (2003). Low-light-adapted Prochlorococcus species possess specific antennae for each photosystem. *Nature*, *424*(6952), 1051–1054.

Bishop, J. K. B., Davis, R. E., & Sherman, J. T. (2002). Robotic observations of dust storm enhancement of carbon biomass in the North Pacific. *Science*, *298*(5594), 817–821.

Björkman, K. M., Church, M. J., Doggett, J. K., & Karl, D. M. (2015). Differential assimilation of inorganic carbon and leucine by Prochlorococcus in the oligotrophic North Pacific subtropical gyre. *Frontiers in Microbiology*, *6*, 1401.

Blain, S., Quéguiner, B., Armand, L., Belviso, S., Bombled, B., Bopp, L., et al. (2007). Effect of natural iron fertilization on carbon sequestration in the Southern Ocean. *Nature*, *446*(7139), 1070–1074.

707 Boiteau, R. M., & Repeta, D. J. (2015). An extended siderophore suite from Synechococcus sp.
708 PCC 7002 revealed by LC-ICPMS-ESIMS. *Metallomics*, *7*(5), 877–884.
709 Boiteau, R. M., Mende, D. R., Hawco, N. J., McIlvin, M. R., Fitzsimmons, J. N., Saito, M. A., et
710 al. (2016). Siderophore-based microbial adaptations to iron scarcity across the eastern
711 Pacific Ocean. *Proceedings of the National Academy of Sciences*, *113*(50), 14237–14242.
712 Boyd, P. W., Jickells, T., Law, C. S., Blain, S., Boyle, E. A., Buesseler, K. O., et al. (2007).
713 Mesoscale iron enrichment experiments 1993-2005: synthesis and future directions.
714 *Science*, *315*(5812), 612–617.
715 Boyle, E. A., Bergquist, B. A., Kayser, R. A., & Mahowald, N. (2005). Iron, manganese, and
716 lead at Hawaii Ocean Time-series station ALOHA: Temporal variability and an
717 intermediate water hydrothermal plume. *Geochimica et Cosmochimica Acta*, *69*(4), 933–
718 952.
719 Browning, T. J., Al-Hashem, A. A., Hopwood, M. J., Engel, A., Belkin, I. M., Wakefield, E. D.,
720 et al. (2021). Iron regulation of North Atlantic eddy phytoplankton productivity.
721 *Geophysical Research Letters*, e2020GL091403.
722 Bruland, K. W., Orians, K. J., & Cowen, J. P. (1994). Reactive trace metals in the stratified
723 central North Pacific. *Geochimica et Cosmochimica Acta*, *58*(15), 3171–3182.
724 Bundy, R. M., Boiteau, R. M., McLean, C., Turk-Kubo, K. A., McIlvin, M. R., Saito, M. A., et
725 al. (2018). Distinct siderophores contribute to iron cycling in the mesopelagic at station
726 ALOHA. *Frontiers in Marine Science*, *5*, 61.
727 Casey, J. R., Lomas, M. W., Mandecki, J., & Walker, D. E. (2007). Prochlorococcus contributes
728 to new production in the Sargasso Sea deep chlorophyll maximum. *Geophysical Research*
729 *Letters*, *34*(10).

730 Cavender-Bares, K. K., Mann, E. L., Chisholm, S. W., Ondrusek, M. E., & Bidigare, R. R.
731 (1999). Differential response of equatorial Pacific phytoplankton to iron fertilization.
732 *Limnology and Oceanography*, *44*(2), 237–246.
733 Chelton, D. B., Schlax, M. G., & Samelson, R. M. (2011). Global observations of nonlinear
734 mesoscale eddies. *Progress in Oceanography*, *91*(2), 167–216.
735 Church, M. J., Ducklow, H. W., Letelier, R. M., & Karl, D. M. (2006). Temporal and vertical
736 dynamics in picoplankton photoheterotrophic production in the subtropical North Pacific
737 Ocean. *Aquatic Microbial Ecology*, *45*(1), 41–53.
738 Church, M. J., Mahaffey, C., Letelier, R. M., Lukas, R., Zehr, J. P., & Karl, D. M. (2009).
739 Physical forcing of nitrogen fixation and diazotroph community structure in the North
740 Pacific subtropical gyre. *Global Biogeochemical Cycles*, *23*(2).
741 Coale, K. H., Fitzwater, S. E., Gordon, R. M., Johnson, K. S., & Barber, R. T. (1996). Control of
742 community growth and export production by upwelled iron in the equatorial Pacific Ocean
743 Kenneth. *Nature*. https://doi.org/10.1038/379621a0
744 Coale, T. H., Moosburner, M., Horák, A., Oborník, M., Barbeau, K. A., & Allen, A. E. (2019).
745 Reduction-dependent siderophore assimilation in a model pennate diatom. *Proceedings of*
746 *the National Academy of Sciences*, *116*(47), 23609–23617.
747 Cullen, J. J. (2015). Subsurface chlorophyll maximum layers: enduring enigma or mystery
748 solved? *Annual Review of Marine Science*, *7*, 207–239.
749 Cunningham, B. R., & John, S. G. (2017). The effect of iron limitation on cyanobacteria major
750 nutrient and trace element stoichiometry. *Limnology and Oceanography*, *62*(2), 846–858.
751 Duhamel, S., Van Wambeke, F., Lefevre, D., Benavides, M., & Bonnet, S. (2018). Mixotrophic
752 metabolism by natural communities of unicellular cyanobacteria in the western tropical

753 South Pacific Ocean. *Environmental Microbiology*, *20*(8), 2743–2756.
754 Ellwood, M. J., Strzepek, R. F., Strutton, P. G., Trull, T. W., Fourquez, M., & Boyd, P. W.
755 (2020). Distinct iron cycling in a Southern Ocean eddy. *Nature Communications*, *11*(1), 1–
756 8.
757 Fitzsimmons, J. N., Hayes, C. T., Al-Subiai, S. N., Zhang, R., Morton, P. L., Weisend, R. E., et
758 al. (2015). Daily to decadal variability of size-fractionated iron and iron-binding ligands at
759 the Hawaii Ocean Time-series Station ALOHA. *Geochimica et Cosmochimica Acta*,
760 *171*(August 2015), 303–324. https://doi.org/10.1016/j.gca.2015.08.012
761 Foreman, R. K., Segura-Noguera, M., & Karl, D. M. (2016). Validation of Ti (III) as a reducing
762 agent in the chemiluminescent determination of nitrate and nitrite in seawater. *Marine*
763 *Chemistry*, *186*, 83–89.
764 Gifford, S. M., Becker, J. W., Sosa, O. A., Repeta, D. J., & DeLong, E. F. (2016). Quantitative
765 transcriptomics reveals the growth-and nutrient-dependent response of a streamlined marine
766 methylotroph to methanol and naturally occurring dissolved organic matter. *MBio*, *7*(6).
767 Hamme, R. C., Webley, P. W., Crawford, W. R., Whitney, F. A., DeGrandpre, M. D., Emerson,
768 S. R., et al. (2010). Volcanic ash fuels anomalous plankton bloom in subarctic northeast
769 Pacific. *Geophysical Research Letters*, *37*(19).
770 Hawco, N. J., Yang, S.-C., Foreman, R. K., Funkey, C. P., Dugenne, M., White, A. E., et al.
771 (2020). Metal isotope signatures from lava-seawater interaction during the 2018 eruption of
772 Kīlauea. *Geochimica et Cosmochimica Acta*, *282*, 340–356.
773 Hawco, N. J., Fu, F., Yang, N., Hutchins, D. A., & John, S. G. (2021). Independent iron and light
774 limitation in a low-light-adapted Prochlorococcus from the deep chlorophyll maximum. *The*
775 *ISME Journal*, *15*(1), 359–362.

776 Hogle, S. L., Dupont, C. L., Hopkinson, B. M., King, A. L., Buck, K. N., Roe, K. L., et al.
777 (2018). Pervasive iron limitation at subsurface chlorophyll maxima of the California
778 Current. *Proceedings of the National Academy of Sciences*, *115*(52), 13300–13305.
779 Hopkinson, B. M., & Barbeau, K. A. (2008). Interactive influences of iron and light limitation on
780 phytoplankton at subsurface chlorophyll maxima in the eastern North Pacific. *Limnology*
781 *and Oceanography*, *53*(4), 1303–1318.
782 Johnson, Z. I., Shyam, R., Ritchie, A. E., Mioni, C., Lance, V. P., Murray, J. W., & Zinser, E. R.
783 (2010). The effect of iron-and light-limitation on phytoplankton communities of deep
784 chlorophyll maxima of the western Pacific Ocean. *Journal of Marine Research*, *68*(2), 283–
785 308.
786 Karl, D. M., Letelier, R. M., Bidigare, R. R., Björkman, K. M., Church, M. J., Dore, J. E., &
787 White, A. E. (2021). Seasonal-to-decadal scale variability in primary production and
788 particulate matter export at Station ALOHA. *Progress in Oceanography*, 102563.
789 Kazamia, E., Sutak, R., Paz-Yepes, J., Dorrell, R. G., Vieira, F. R. J., Mach, J., et al. (2018).
790 Endocytosis-mediated siderophore uptake as a strategy for Fe acquisition in diatoms.
791 *Science Advances*, *4*(5), eaar4536.
792 Letelier, R. M., Bidigare, R. R., Hebel, D. V, Ondrusek, M., Winn, C. D., & Karl, D. M. (1993).
793 Temporal variability of phytoplankton community structure based on pigment analysis.
794 *Limnology and Oceanography*, *38*(7), 1420–1437.
795 Letelier, R. M., Karl, D. M., Abbott, M. R., & Bidigare, R. R. (2004). Light driven seasonal
796 patterns of chlorophyll and nitrate in the lower euphotic zone of the North Pacific
797 Subtropical Gyre. *Limnology and Oceanography*, *49*(2), 508–519.
798 Lis, H., Shaked, Y., Kranzler, C., Keren, N., & Morel, F. M. M. (2015). Iron bioavailability to

799 phytoplankton: an empirical approach. *The ISME Journal*, *9*(4), 1003–1013.
800 Lorenzen, C. J. (1967). Determination of chlorophyll and pheo-pigments: spectrophotometric
801 equations 1. *Limnology and Oceanography*, *12*(2), 343–346.
802 Maldonado, M. T., & Price, N. M. (1996). Influence of N substrate on Fe requirements of marine
803 centric diatoms. *Marine Ecology Progress Series*, *141*, 161–172.
804 Maldonado, M. T., & Price, N. M. (1999). Utilization of iron bound to strong organic ligands by
805 plankton communities in the subarctic Pacific Ocean. *Deep Sea Research Part II: Topical*
806 *Studies in Oceanography*, *46*(11–12), 2447–2473.
807 Maldonado, M. T., & Price, N. M. (2001). Reduction and transport of organically bound iron by
808 Thalassiosira oceanica (Bacillariophyceae). *Journal of Phycology*, *37*(2), 298–310.
809 Malmstrom, R. R., Coe, A., Kettler, G. C., Martiny, A. C., Frias-Lopez, J., Zinser, E. R., &
810 Chisholm, S. W. (2010). Temporal dynamics of Prochlorococcus ecotypes in the Atlantic
811 and Pacific oceans. *The ISME Journal*, *4*(10), 1252.
812 Mann, E. L., & Chisholm, S. W. (2000). Iron limits the cell division rate of Prochlorococcus in
813 the eastern equatorial Pacific. *Limnology and Oceanography*, *45*(5), 1067–1076.
814 Marchetti, A., Maldonado, M. T., Lane, E. S., & Harrison, P. J. (2006). Iron requirements of the
815 pennate diatom Pseudo-nitzschia: Comparison of oceanic (high-nitrate, low-chlorophyll
816 waters) and coastal species. *Limnology and Oceanography*, *51*(5), 2092–2101.
817 Martin, J H, Coale, K. H., Johnson, K. S., Fitzwater, S. E., Gordon, R. M., Tanner, S. J., et al.
818 (1994). Testing the iron hypothesis in ecosystems of the equatorial Pacific Ocean. *Nature*,
819 *371*, 123.
820 Martin, John H, Gordon, R. M., & Fitzwater, S. E. (1990). Iron in Antarctic waters. *Nature*,
821 *345*(6271), 156–158.

822 McGillicuddy Jr, D. J. (2016). Mechanisms of physical-biological-biogeochemical interaction at
823 the oceanic mesoscale.
824 Mignot, A., Claustre, H., Uitz, J., Poteau, A., d'Ortenzio, F., & Xing, X. (2014). Understanding
825 the seasonal dynamics of phytoplankton biomass and the deep chlorophyll maximum in
826 oligotrophic environments: A Bio-Argo float investigation. *Global Biogeochemical Cycles*,
827 *28*(8), 856–876.
828 Moore, C. M., Mills, M. M., Arrigo, K. R., Berman-Frank, I., Bopp, L., Boyd, P. W., et al.
829 (2013). Processes and patterns of oceanic nutrient limitation. *Nature Geoscience*, *6*(9), 701–
830 710.
831 Moore, J. K., Doney, S. C., Glover, D. M., & Fung, I. Y. (2001). Iron cycling and nutrient-
832 limitation patterns in surface waters of the World Ocean. *Deep Sea Research Part II:*
833 *Topical Studies in Oceanography*, *49*(1–3), 463–507.
834 Moore, L. R., Post, A. F., Rocap, G., & Chisholm, S. W. (2002). Utilization of different nitrogen
835 sources by the marine cyanobacteria Prochlorococcus and Synechococcus. *Limnology and*
836 *Oceanography*, *47*(4), 989–996.
837 Morel, F. M. M., Hudson, R. J. M., & Price, N. M. (1991). Limitation of productivity by trace
838 metals in the sea. *Limnology and Oceanography*, *36*(8), 1742–1755.
839 Morel, F. M. M., Kustka, A. B., & Shaked, Y. (2008). The role of unchelated Fe in the iron
840 nutrition of phytoplankton. *Limnology and Oceanography*, *53*(1), 400–404.
841 Pollard, R. T., Salter, I., Sanders, R. J., Lucas, M. I., Moore, C. M., Mills, R. A., et al. (2009).
842 Southern Ocean deep-water carbon export enhanced by natural iron fertilization. *Nature*,
843 *457*(7229), 577–580.
844 Price, N. M., Ahner, B. A., & Morel, F. M. M. (1994). The equatorial Pacific Ocean: Grazer-

controlled phytoplankton populations in an iron-limited ecosystem 1. *Limnology and Oceanography*, *39*(3), 520–534.

Raven, J. A. (1988). The iron and molybdenum use efficiencies of plant growth with different energy, carbon and nitrogen sources. *New Phytologist*, *109*(3), 279–288.

Raven, J. A. (1990). Predictions of Mn and Fe use efficiencies of phototrophic growth as a function of light availability for growth and of C assimilation pathway. *New Phytologist*, *116*(1), 1–18.

Sedwick, P N, Bowie, A. R., Church, T. M., Cullen, J. T., Johnson, R. J., Lohan, M. C., et al. (2020). Dissolved iron in the Bermuda region of the subtropical North Atlantic Ocean: Seasonal dynamics, mesoscale variability, and physicochemical speciation. *Marine Chemistry*, 103748.

Sedwick, Peter N, Church, T. M., Bowie, A. R., Marsay, C. M., Ussher, S. J., Achilles, K. M., et al. (2005). Iron in the Sargasso Sea (Bermuda Atlantic Time-series Study region) during summer: Eolian imprint, spatiotemporal variability, and ecological implications. *Global Biogeochemical Cycles*, *19*(4).

Shire, D. M., & Kustka, A. B. (2015). Luxury uptake, iron storage and ferritin abundance in Prochlorococcus marinus (Synechococcales) strain MED4. *Phycologia*, *54*(4), 398–406.

Siegel, D. A., McGillicuddy Jr, D. J., & Fields, E. A. (1999). Mesoscale eddies, satellite altimetry, and new production in the Sargasso Sea. *Journal of Geophysical Research: Oceans*, *104*(C6), 13359–13379.

Strickland, J. D. H., & Parsons, T. R. (1972). A practical handbook of seawater analysis.

Strong, A., Chisholm, S., Miller, C., & Cullen, J. (2009). Ocean fertilization: time to move on. *Nature*, *461*(7262), 347–348.

868 Strzepek, R. F., Hunter, K. A., Frew, R. D., Harrison, P. J., & Boyd, P. W. (2012). Iron-light
869 interactions differ in Southern Ocean phytoplankton. *Limnology and Oceanography*, *57*(4),
870 1182–1200.
871 Sunda, W., Price, N., Morel, F., Service, N. O., & Road, P. I. (2005). Trace metal ion buffers and
872 their use in culture studies. In *Algal Culturing Techniques* (pp. 35–63). Academic Press.
873 Sunda, W. G., & Huntsman, S. A. (1997). Interrelated influence of iron, light and cell size on
874 marine phytoplankton growth. *Nature*, *390*(6658), 389–392.
875 Thompson, A. W., Huang, K., Saito, M. A., & Chisholm, S. W. (2011). Transcriptome response
876 of high- and low-light-adapted Prochlorococcus strains to changing iron availability. *The*
877 *Isme Journal*, *5*, 1580. Retrieved from http://dx.doi.org/10.1038/ismej.2011.49
878 Virtanen, P., Gommers, R., Oliphant, T. E., Haberland, M., Reddy, T., Cournapeau, D., et al.
879 (2020). SciPy 1.0: fundamental algorithms for scientific computing in Python. *Nature*
880 *Methods*, *17*(3), 261–272.
881 Viviani, D. A., & Church, M. J. (2017). Decoupling between bacterial production and primary
882 production over multiple time scales in the North Pacific Subtropical Gyre. *Deep Sea*
883 *Research Part I: Oceanographic Research Papers*, *121*, 132–142.
884 Ward, B. A., Dutkiewicz, S., Moore, C. M., & Follows, M. J. (2013). Iron, phosphorus, and
885 nitrogen supply ratios define the biogeography of nitrogen fixation. *Limnology and*
886 *Oceanography*, *58*(6), 2059–2075.
887 Wilson, S. T., Aylward, F. O., Ribalet, F., Barone, B., Casey, J. R., Connell, P. E., et al. (2017).
888 Coordinated regulation of growth, activity and transcription in natural populations of the
889 unicellular nitrogen-fixing cyanobacterium Crocosphaera. *Nature Microbiology*, *2*(9), 1–9.
890 Wilson, S. T., Hawco, N. J., Armbrust, E. V., Barone, B., Björkman, K. M., Boysen, A. K., et al.

(2019). Kīlauea lava fuels phytoplankton bloom in the North Pacific Ocean. *Science*, *365*(6457), 1040 LP – 1044.

Wu, J., Sunda, W., Boyle, E. A., & Karl, D. M. (2000). Phosphate Depletion in the Western North Atlantic Ocean. *Science*, *289*(5480), 759 LP – 762.

Wunsch, C. (1997). The vertical partition of oceanic horizontal kinetic energy. *Journal of Physical Oceanography*, *27*(8), 1770–1794.

Zhang, Z., Wang, W., & Qiu, B. (2014). Oceanic mass transport by mesoscale eddies. *Science*, *345*(6194), 322–324.

914 **Table 1.** Attributes of the DCM in the cyclonic and anticyclonic eddies observed during the 2017
915 MESO-SCOPE expedition. Values in italics derive from the Lagrangian observation period at
916 the eddy centers. May – September average values from Station ALOHA are shown for
917 comparison.

Parameter	MESO-SCOPE, June – July 2017 Cyclone	Anticyclone	HOT, May – September Station ALOHA[a]
Latitude, Longitude (°N, °W)	24.86, 158.57	26.37, 158.01	22.75, 158.0
Sea level anomaly (SLA_{corr}, cm)	-18	+25	+0.9
Density (σ_θ, kg m^{-3})	*25.22*	*24.37*	24.23 – 24.67
Mean Isopycnal Depth (m)	104	118	100 – 125
Chlorophyll *a* (μg L^{-1})	0.32 (*0.30*)	0.19 (*0.24*)	0.19 – 0.21
Light (PAR, mol photon m^{-2} day^{-1})	*0.46 ± 0.18*	*0.29 ± 0.02*	0.5[b] (0.23 – 0.74[a])
Primary production (μM C day^{-1})	0.21	0.10	0.12 ± 0.04[c] (0.07 – 0.21[a])
Nitrate + Nitrite (nM)	820	3	25 – 233
Nitrite (nM)	79	< 3	2 – 45
Phosphate (nM)	168 (*145*)	85 (*77*)	62 – 93
Silicate (nM)	3,300	1,900	1,380 – 1,580
Dissolved Iron (dFe, pM)	63	136	66 ± 21[d]
Dissolved Mn (pM)	620	1,390	1,250[e]
dFe:NO_3 supply ratio (μmol:mol)[f]	50.4	215	87.4 – 100
Picoeukaryotes (cells ml^{-1})	*4,050*	*2,280*	1,200 – 1,200
Prochlorococcus (cells ml^{-1})	*57,600*	*79,000*	67,000 – 155,000
Heterotrophic bacteria (cells ml^{-1})	*485,000*	*406,000*	314,000 – 387,000

[a] Average values at 100 m and 125 m obtained from the HOT-DOGS online database.
[b] Letelier et al. (2004)
[c] Average for all month/depth combinations with an irradiance between 0.2 – 0.6 mol photon m^{-2} day^{-1}.
[d] Obtained from Fitzsimmons et al. (2015), averaged over 90-130 m depth range.
[e] Boyle et al. (2005) from MP5 cruise (July 1, 2002).
[f] Calculated as the sum of upward (DCM to 250 m) and downward (surface to DCM) dFe/dz relative to upward (DCM to 250 m) dNO_3/dz, assuming similar diffusive mixing above and below the DCM.

925
926
927
928
929
930
931
932
933
934
935
936
937
938
939
940
941
942
943

Table 2. Abundance of *Prochlorococcus* nutrient stress gene markers based on transcriptomes from the DCM of both eddies. The ratio of transcripts in the cyclonic versus anticyclonic eddies (C:A Ratio) is shown after normalization to total *Prochlorococcus* transcripts.

Gene product	Expected iron stress response?	Mean DCM expression (copies ml^{-1})		Normalized C:A Ratio
		Cyclone	Anticyclone	
Fe binding protein (*idiA*, COG1840)	Upregulation[1]	14,000	9,900	1.17
Flavodoxin (*isiB*, COG0716)	Upregulation[1]	77,000	60,000	1.08
Ferredoxin (*petF*, COG0633)	Downregulation[1]	6,800	10,400	0.54*
Ferritin (COG1528)	Downregulation[2]	15,000	14,000	0.89
Photosystem II D1 (*psbA*, ENOG502Z87P)		520,000	510,000	0.86

[1]Significantly regulated in *Prochlorococcus* MED4 and *Prochlorococcus* MIT9313, Thompson et al. (2011)
[2]Shire and Kutska, 2015
*Corrected p-value < 0.05

Global Biogeochemical Cycles

Supporting Information for

Mesoscale eddies as natural iron fertilization experiments to the deep chlorophyll maximum

Nicholas J. Hawco[1,2], Benedetto Barone[2], Matthew J. Church[3], Lydia Babcock-Adams[4], Daniel J. Repeta[4], Emma K. Wear[3], Rhea K. Foreman[2], Karin M. Björkman[2], Shavonna Bent[4], Benjamin A. S. Van Mooy[4], Uri Sheyn[2], Edward F. Delong[2], Marianne Acker[4], Rachel L. Kelley[1], Alex Nelson[2], John Ranieri[3], Tara Clemente[2], David M. Karl[2], and Seth G. John[1]

[1]Department of Earth Sciences, University of Southern California, Los Angeles, CA USA.

[2]Department of Oceanography, University of Hawaii at Mānoa, Honolulu, HI, USA.

[3]Flathead Lake Biological Station, University of Montana, Polson, MT, USA.

[4]Woods Hole Oceanographic Institution, Woods Hole, MA, USA.

Contents of this file

Supplemental Methods

16S rRNA amplicon sequencing

Genomic DNA was extracted from filters collected from the long-term incubations as described in the main text. Samples were lysed by freeze-thawing and bead-beating in a Biospec Mini-Beadbeater-16, then DNA was extracted using the MasterPure Complete DNA and RNA Purification Kit (Lucigen). Genomic DNA was quantitated using a Qubit v4 with High-Sensitivity DNA Kit.

Bacterioplankton community composition was assessed by sequencing 16S rRNA gene amplicons using primers targeting the V4-V5 hypervariable region: 515F-Y, 5'-GTGYCAGCMGCCGCGGTAA-3', and 926-R, 5'-CCGYCAATTYMTTTRAGTTT-3', as recommended by Parada et al. (2016) and with multiplexing indexes as designed by the Earth Microbiome Project (Caporaso et al. 2012). Triplicate 25 µL PCR reactions consisted of: 10 µL 2x Invitrogen Platinum II Hot-Start PCR Master Mix, 0.5 µL, 10 µM indexed forward primer (515F-Y), 0.5 µL, 10 µM reverse primer (926R), 12 µL PCR water (Invitrogen Ultra Pure Distilled Water), and 2 µL genomic DNA. PCR reactions were cycled in a Bio-Rad Tetrad 2 thermal cycler on the following program: 1) 94° C, 2 hr; 2) 35 cycles of: 94° C, 45 min, 58° C, 1hr, 72° C, 1.5 hr; 3) 72° C, 10 hr. Pooled triplicate amplicons were visually verified on an agarose gel, cleaned with an ENZA Cycle Pure Kit (Omega Bio-tek), quantitated using a Qubit v3 with High-Sensitivity DNA Kit, and pooled at equimolar proportions. The pooled library was sequenced using an Illumina MiSeq with PE250 v2 chemistry at the University of Montana Genomics Core.

Amplicon sequence variants (ASVs) were generated in DADA2 v1.14.1 (Callahan et al. 2016) and classified using the SILVA v138 database (Quast et al. 2013). Sequences identified as plastids, mitochondria, and eukaryotes were removed. Samples were subsampled to 20,000 sequences using the "rrarefy" function in the R package vegan (Oksanen et al. 2019). Sequences were aligned using the R package DECIPHER (Wright 2016); aligned sequences were used to generate a phylogenetic tree using the R package phangorn (Schliep 2011); and a weighted UniFrac distance matrix (Lozupone and Knight 2005) was calculated using the R package phyloseq (McMurdie and Holmes 2013). Multivariate statistics were conducted in Primer-E v6 (Clarke and Gorley 2006). Full bioinformatics code and ASV results are available at: https://github.com/ekwear/AlohaFe16S

Transcriptomics

Approximately 1 L of seawater for metatranscriptomic samples was filtered onto a 0.2 µm Supor® Membrane Disc filters (Pall) housed in SwinnexTM filter manifolds (MilliporeSigma) using a peristaltic pump. The filtration time ranged from 15 to 20 min. Immediately following filtration, filters were placed in RNALater (Invitrogen, Waltham, MA, USA) and stored at -80°C until processing.

RNA extractions were performed by first removing RNALater (via centrifugation and pipetting), adding 300 µL of Ambion denaturing solution directly onto the filter, and spiking in External RNA Controls Consortium (ERCC) ExFold RNA Spike-In Mixes (Mix #1, 4456739 , Invitrogen) followed by vortexing for 1 min. 750 µL of nuclease-free water was added to the sample, which were then purified and DNase-treated using a Chemagen MSM I instrument with the tissue RNA CMG-1212A kit (PerkinElmer). Samples were enriched for mRNA by removal of rRNA using Ribozero (Illumina, San Diego, CA, USA). The quality of purified RNA was assessed using Fragment Analyzer high sensitivity reagents (Agilent, Santa Clara, CA, USA) and quantified using Ribogreen (Invitrogen). cDNA was synthesized and sequencing libraries were produced using the ScriptSeq v2 RNA-Seq kit (Illumina #SSV21124). Unique single-plex barcodes were annealed onto cDNA fragments during the PCR enrichment for Illumina sequencing primers over

12 cycles, following the manufacturer's guidelines. Libraries were normalized to 4 nmol L^{-1} final DNA concentration, pooled in equal volumes, and sequenced using an Illumina® NextSeq 500 system with a V2 high output 300 cycle reagent kit. A phiX quality control (Illumina) reagent was added to an estimated final contribution of 5% of the total estimated sequence density. A total of ~2 million, 150 bp paired-end reads were produced for each sample.

Sequence reads were verified and screened for quality using BBMap (v38.73, www.sourceforge.net/projects/bbmap/) to remove adapters and phiX, BFC r181 (Li, 2015) to correct sequencing errors, and Trimmomatic v0.39 (Bolger et al., 2014)) to remove low quality bases. Raw sequence reads were submitted to the NCBI SRA under project number PRJNA596510. Cleaned reads were assembled using RNA-SPAdes v3.13.2 (Bushmanova et al., 2019), and genes were predicted from assembled transcripts using Prodigal v2.6.3 (Hyatt et al., 2010). A combined gene database was created from predicted genes and the ALOHA 2.0 gene catalog (Luo et al., 2020) using CD-HIT v4.8.1 (Fu et al., 2012) to dereplicate genes at a 97% amino acid identity cutoff. Transcripts were identified and counted by mapping cleaned reads against this combined gene catalog using BWA-MEM (v0.7.17, www.github.com/lh3/bwa). Transcript counts were normalized to the ERCC standards to account for any methodological biases, including library preparation and sequencing, between samples.

Transcript counts were normalized to the volume of water filtered for each sample to calculate transcripts per mL for each gene. To use the ERCC spike-in as an internal standard in each sample, the correction factor was calculated as follows: for each ERCC standard, the known quantities of spiked-in RNA standards were compared to that same standard's read counts recovered by read mapping using BBMap (v38.73, www.sourceforge.net/projects/bbmap/). A standard curve was generated for each sample, and the corresponding correction factor calculated as the slope of the best fit line going through these pairs of values with the intersection forced to the origin. The detection limit corresponded to the lowest molar amount of the ERCC sequence detectable in each sample. Values above detection limits were further normalized to the total sample expression sum of each specific genus level annotation, using GTDB (Parks et al., 2018) to identify prokaryote transcripts. This step was required in order to compare eddy differential gene expression based on cellular regulation rather than the total number of cells.

Supplemental References

Bolger, A. M., Lohse, M., & Usadel, B. (2014). Trimmomatic: a flexible trimmer for Illumina sequence data. *Bioinformatics*, *30*(15), 2114–2120.

Bushmanova, E., Antipov, D., Lapidus, A., & Prjibelski, A. D. (2019). rnaSPAdes: a de novo transcriptome assembler and its application to RNA-Seq data. *GigaScience*, *8*(9), giz100.

Callahan, B.J., P.J. McMurdie, M.J. Rosen, A.W. Han, A.J.A. Johnson, and S.P. Holmes. 2016. DADA2: High-resolution sample inference from Illumina amplicon data. Nature Methods 13: 581-583. doi: 10.1038/nmeth.3869

Caporaso, J.G, C.L. Lauber, W.A. Walters, D. Berg-Lyons, J. Huntley, N. Fierer, S.M. Owens, J. Betley, L. Fraser, M. Bauer, N. Gormley, J.A. Gilbert, G. Smith, and R. Knight. 2012. Ultra-high-throughput microbial community analysis on the Illumina HiSeq and MiSeq platforms. The ISME J 6: 1621-1624. doi: 10.1038/ismej.2012.8

Clarke, K.R., and R.N. Gorley. 2006. PRIMER v6: user manual/tutorial. New Brunswick, Canada: PRIMER-E.

Fu, L., Niu, B., Zhu, Z., Wu, S., & Li, W. (2012). CD-HIT: accelerated for clustering the next-generation sequencing data. *Bioinformatics*, *28*(23), 3150–3152.

Hyatt, D., Chen, G.-L., LoCascio, P. F., Land, M. L., Larimer, F. W., & Hauser, L. J. (2010). Prodigal: prokaryotic gene recognition and translation initiation site identification. *BMC Bioinformatics*, *11*(1), 1–11.

Li, H. (2015). BFC: correcting Illumina sequencing errors. *Bioinformatics*, *31*(17), 2885–2887.

Lozupone, C., and R. Knight. 2005. UniFrac: a new phylogenetic method for comparing microbial communities. Appl. Environ. Microbiol. 71: 8228-8235. doi: 10.1128/AEM.71.12.8228-8235.2005

Luo, E., Eppley, J. M., Romano, A. E., Mende, D. R., & DeLong, E. F. (2020). Double-stranded DNA virioplankton dynamics and reproductive strategies in the oligotrophic open ocean water column. *The ISME Journal*, *14*(5), 1304–1315.

McMurdie, P.J., and S. Holmes. 2013. phyloseq: An R package for reproducible interactive analysis and graphics of microbiome census data. PloS ONE 8: e61217. doi: 10.1371/journal.pone.0061217

Oksanen, J., F.G. Blanchet, M. Friendly, R. Kindt, P. Legendre, D. McGlinn, P.R. Minchin, R.B. O'Hara, G.L. Simpson, P. Solymos, M.H.M. Stevens, E. Szoecs, and H. Wagner. 2019. vegan: Community ecology package. R package version 2.5-6. https://CRAN.R-project.org/package=vegan

Parada, A.E., D.M. Needham, and J.A. Fuhrman. 2016. Every base matters: assessing small subunit rRNA primers for marine microbiomes with mock communities, time series and global field samples. Environmental Microbiology 18: 1403-1414. doi: 10.1111/1462-2920.13023

Parks, D. H., Chuvochina, M., Waite, D. W., Rinke, C., Skarshewski, A., Chaumeil, P.-A., & Hugenholtz, P. (2018). A standardized bacterial taxonomy based on genome phylogeny substantially revises the tree of life. *Nature Biotechnology*, *36*(10), 996–1004.

Quast, C., E. Pruesse, P. Yilmaz, J. Gerken, T. Schweer, P. Yarza, J. Peplies, F.O. Glöckner. 2013. The SILVA ribosomal RNA gene database project: improved data processing and web-based tools. Nucleic Acids Res. 41: D590-D596. doi:10.1093/nar/gks1219

Schliep, K.P. 2011. phangorn: phylogenetic analysis in R. Bioinformatics 27: 592-593. doi: 10.1093/bioinformatics/btq706

Wright, E.S. 2016. Using DECIPHER v2.0 to analyze big biological sequence data in R. The R Journal 8: 352-359.

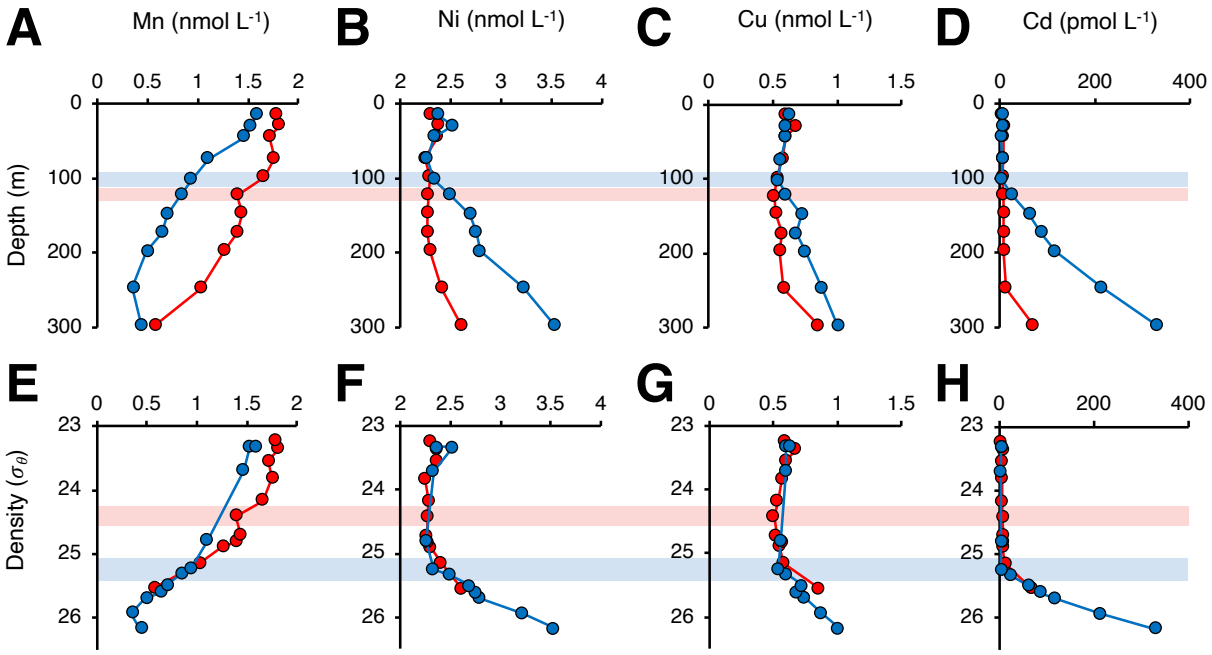

Figure S1. Density driven variation in Mn (a, e), Ni (b, f), Cu (c, g) and Cd (d, h) for the cyclonic eddy (blue) and anticyclonic eddy (red). Top panels (a-d) are plotted against depth and bottom panels (e-h) are plotted against potential density with the DCM layers for each eddy highlighted in blue and red shading. See Fig. 3 in the main text.

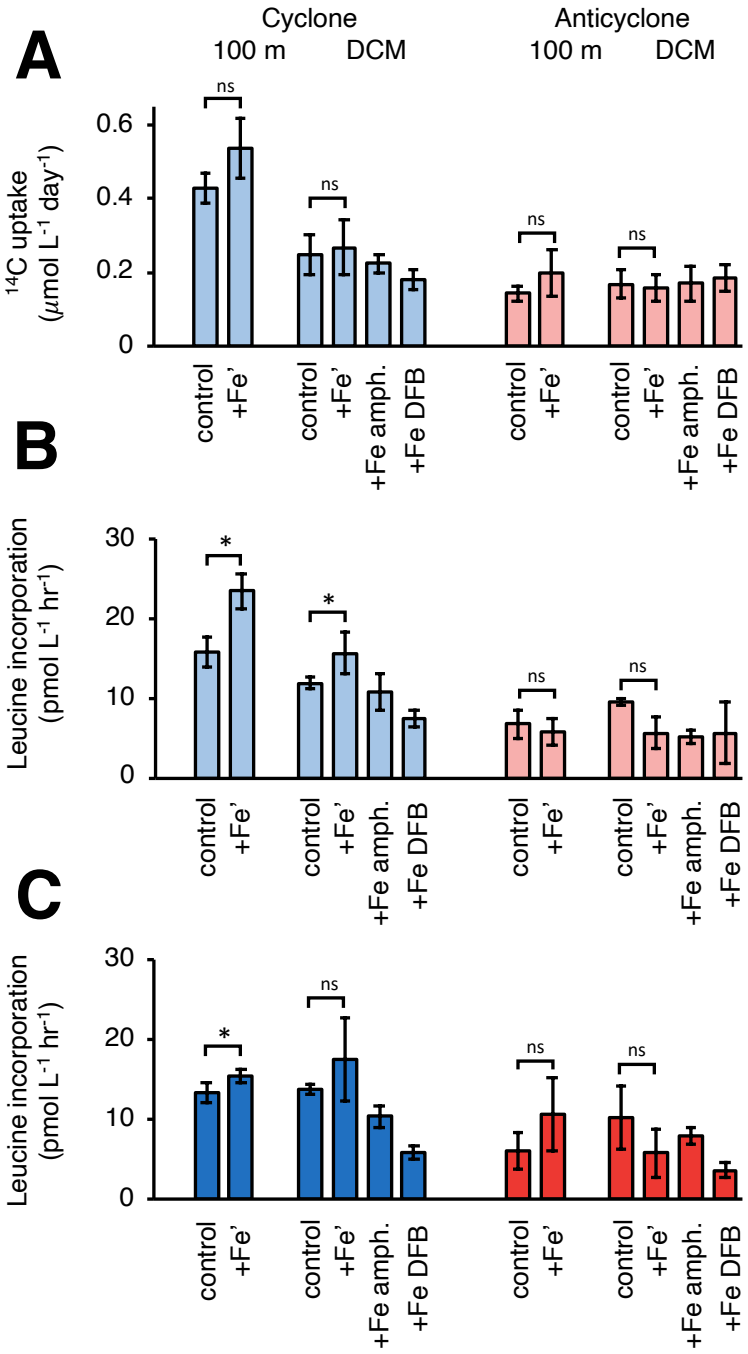

Figure S2. Fe addition experiments at 100 m and the DCM. ^{14}C primary production (a) and leucine incorporation under ambient light (b) and in darkness (c) for the cyclonic eddy (blue) and anticyclonic eddy (red). Statistical comparisons for 'control' and '+Fe' treatments reflect pairwise comparisons (Student's t-test) at 100 m and one way ANOVAs with Fisher least significant difference (LSD) tests for DCM experiments (light and dark experiments considered separately). Asterisks (*) denote $p < 0.05$, 'ns' denotes $p > 0.05$.

Table S1. Isopycnal analysis of biogeochemical parameters with SLA_{corr} at Station ALOHA using the analyses of Barone et al. (2019). Median values for each bin are shown for all fields. NA reflects no measurements available.

24.50

SLA bin cm	SLA cm	Depth m	NO_3 μmol L^{-1}	Si μmol L^{-1}	$Si - NO_3$ μmol L^{-1}	Chl μg L^{-1}	O_2 μmol L^{-1}	^{14}C uptake μmol L^{-1} day^{-1}
< -10	-13.4	99	0.04	1.53	1.368	0.19	217	0.28
-10 to -5	-7.3	102	0.19	1.57	1.323	0.19	214	0.12
-5 to -1'	-3.5	122	0.30	1.53	1.1695	0.21	208	0.14
-1 to +1'	-0.1	125	0.54	1.59	1.0835	0.16	204	0.07
+1 to +5	3.4	132	0.57	1.70	1.1665	0.13	206	0.06
+5 to +10	7.2	149	0.65	1.57	0.962	0.11	203	0.07
> +10	12.8	157	0.60	1.75	1.092	0.08	202	0.04
> +10	12.8	213	2.51	2.88	0.56	0.01	197	NA

24.75

SLA bin cm	SLA cm	Depth m	NO_3 μmol L^{-1}	Si μmol L^{-1}	$Si - NO_3$ μmol L^{-1}	Chl μg L^{-1}	O_2 μmol L^{-1}	^{14}C uptake μmol L^{-1} day^{-1}
< -10	-13.4	125	0.52	1.81	1.38	0.20	209	0.13
-10 to -5	-7.3	131	0.85	1.88	0.99	0.12	204	0.10
-5 to -1'	-3.5	144	1.18	1.91	0.80	0.10	202	0.06
-1 to +1'	-0.1	151	1.26	2.04	0.75	0.06	200	0.03
+1 to +5	3.4	166	1.34	2.09	0.82	0.05	200	0.00
+5 to +10	7.2	175	1.31	2.01	0.66	0.04	197	NA
> +10	12.8	188	1.33	2.24	0.73	0.04	198	NA

25.00

SLA bin cm	SLA cm	Depth m	NO_3 μmol L^{-1}	Si μmol L^{-1}	$Si - NO_3$ μmol L^{-1}	Chl μg L^{-1}	O_2 μmol L^{-1}	^{14}C uptake μmol L^{-1} day^{-1}
< -10	-13.4	150	1.72	2.45	0.75	0.07	201	0.01
-10 to -5	-7.3	164	1.88	2.64	0.51	0.04	200	0.01
-5 to -1'	-3.5	175	2.19	2.50	0.40	0.04	198	NA
-1 to +1'	-0.1	177	2.30	2.73	0.34	0.02	196	0.01
+1 to +5	3.4	200	2.41	2.66	0.32	0.02	195	NA
+5 to +10	7.2	201	2.27	2.70	0.26	0.02	196	NA
> +10	12.8	213	2.51	2.88	0.56	0.01	197	NA